University of Reading

A comparative study on design and performance evaluation of Organic Rankine Cycle (ORC) under different two-phase heat transfer correlations

Article

Published Version

Creative Commons: Attribution 4.0 (CC-BY)

Open Access

Zhang, Ji, Hu, Xudong, Wu, Ding, Huang, Xiaohui, Wang, Xuehui, Yang, Yan and Wen, Chuang ORCID logoORCID: https://orcid.org/0000-0002-4445-1589 (2023) A comparative study on design and performance evaluation of Organic Rankine Cycle (ORC) under different two-phase heat transfer correlations. Applied Energy, 350. 121724. ISSN 03062619 doi: https://doi.org/10.1016/j.apenergy.2023.121724 Available at https://centaur.reading.ac.uk/112929/

It is advisable to refer to the publisher's version if you intend to cite from the work. See Guidance on citing.
Published version at: http://dx.doi.org/10.1016/j.apenergy.2023.121724
To link to this article DOI: http://dx.doi.org/10.1016/j.apenergy.2023.121724

Publisher: Elsevier

All outputs in CentAUR are protected by Intellectual Property Rights law, including copyright law. Copyright and IPR is retained by the creators or other copyright holders. Terms and conditions for use of this material are defined in the End User Agreement.

University of Reading

www.reading.ac.uk/centaur

CentAUR

Central Archive at the University of Reading

Reading's research outputs online

Applied Energy 350 (2023) 121724

Contents lists available at ScienceDirect

Applied Energy

journal homepage: www.elsevier.com/locate/apenergy

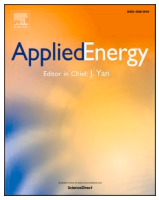

A comparative study on design and performance evaluation of Organic Rankine Cycle (ORC) under different two-phase heat transfer correlations

Ji Zhang [a], Xudong Hu [a], Ding Wu [a,*], Xiaohui Huang [a,*], Xuehui Wang [b], Yan Yang [c,*], Chuang Wen [c,d,*]

[a] School of Electrical and Information Engineering, Hunan University, Changsha 410082, China
[b] Chemical Engineering Department, Imperial College London, London SW7 2AZ, UK
[c] Faculty of Environment, Science and Economy, University of Exeter, Exeter EX4 4QF, UK
[d] School of the Built Environment, University of Reading, Reading RG6 6AH, UK

HIGHLIGHTS

- 8 two-phase heat transfer correlations are compared for designing the heat exchangers.
- Designed condensers are affected by the heat transfer correlations more significantly.
- Net output power is slightly influenced with a relative difference within 1.1%.
- Electricity production cost is affected with a relative difference 11.2%.
- Total carbon emissions exhibit minimal variation with a relative difference of only 0.96%.

ARTICLE INFO

Keywords:
Low-grade heat
Organic Rankine cycle (ORC)
Plate heat exchanger
Correlation
Heat transfer
Off-design

ABSTRACT

Organic Rankine cycle (ORC) is considered to be a good solution to the high-efficient recovery of low-grade heat for saving energy and reducing carbon emissions. As the core component, the heat exchanger plays a significant role in the thermo-economic performance evaluation of an ORC plant and its heat transfer correlations greatly influence the cycle performance. In this paper, 8 two-phase heat transfer correlations (4 flow boiling ones and 4 flow condensation ones) are utilized to design the plate-type heat exchangers, and a comparative study among different correlations is carried out. The result shows the designed evaporators are finitely affected by heat transfer correlations whereas the situation with the designed condensers is the opposite. The net output power is slightly influenced with a relative difference within 1.1% but the system's economic performance is significantly affected with the maximum relative difference of electricity production cost up to 11.2%. The environmental performance is hardly affected by correlations with the maximum relative difference of total greenhouse gas emission within 0.96%. This paper analyzed the performance variation of the ORC under different correlations and provided a guideline for designing heat exchangers and evaluating the off-design performance of ORC systems.

1. Introduction

Energy especially electricity plays a significant role in modern society and fossil fuel is still the main energy source, which has limited reserves and pollutes the environment. High-efficient utilization of low-grade heat such as solar, geothermal, and industrial waste heat sources is of great importance for alleviating the shortage of energy and reducing carbon emissions at the same time. Owing to the simple structure, easy maintenance, low cost, and moderate operating pressures, the organic Rankine cycle (ORC) is commonly accepted as a feasible way to convert low-grade heat into electric power [1,2]. According to the existing literature, 70% to 90% of the total exergy loss of the ORC system happens in the heat exchangers. Also, the investment cost for the heat exchangers roughly occupies 29.2% - 34.1% of the gross investment for the ORC system [3]. Due to the high irreversible heat loss and investment cost, the heat exchanger used in the ORC system is an important factor in the system's efficiency and economy [4,5].

* Corresponding authors.
E-mail addresses: dingwu@hnu.edu.cn (D. Wu), xiaohuih@hnu.edu.cn (X. Huang), y.yang7@exeter.ac.uk (Y. Yang), c.wen@reading.ac.uk (C. Wen).

https://doi.org/10.1016/j.apenergy.2023.121724
Received 25 May 2023; Received in revised form 8 July 2023; Accepted 2 August 2023
Available online 10 August 2023
0306-2619/© 2023 The Author(s). Published by Elsevier Ltd. This is an open access article under the CC BY license (http://creativecommons.org/licenses/by/4.0/).

Nomenclature

Abbreviations

CO_2	Carbon dioxide
EPC	Electricity production cost
GHG	Greenhouse gas
ORC	Organic Rankine cycle
PHE	Plate heat exchanger

Variables

b	Plate corrugation depth (mm)
Bo	Boiling number (−)
s	Cost ($)
Co	Convection number (−)
d	Diameter (m)
f	Correction coefficient (−)
Fr	Froude number (−)
g	Gravitational acceleration (m/s^2)
G	Mass flux (kg/(s·m^2))
Ge	Geometric parameters (−)
h	Enthalpy (kJ/kg)
I	Exergy (kW)
k	Thermal conductivity (W/(m·°C))
L	Length (m)
m	Mass flow (kg/s)
M	Molar mass (g/mol)
Nu	Nusselt number (−)
p	Pressure (kPa)
Pr	Prandtl number (−)
P_r	Reduced pressure (−)
Q	Heat transfer rate (kW)
Re	Reynolds number (−)
s	Entropy (kJ/(mol·°C))
t	Plate thickness (mm)
T	Temperature (°C)
w	Plate width (m)
W	Power (kW)
x	Vapour quality (−)
X	Corrugation parameter (−)
X_{tt}	Lockhart-Martinelli parameter (−)
α	Heat transfer coefficient (W/(m^2·°C))
β	Plate chevron angle (°)
η	Efficiency (−)
λ	Plate corrugation wavelength (mm)
μ	Dynamic viscosity (Pa·s)
ρ	Density (kg/m^3)
σ	Surface tension (N)
φ	Area-enlargement factor (−)

Superscript and subscript

ave	Average
cond	Condensation
cs	Cold source
eq	Equivalent
eva	Evaporation
h	Hydraulic
hs	Heat source
in	Inlet
l	Liquid
net	Net output
out	Outlet
pool	Pool boiling
sp	Single phase
tp	Two-phase
v	Vapour
Δ	Difference

Therefore, the precision design for the heat exchangers plays a significant role in improving the thermo-economic performance of the ORC system.

Among different types of heat exchangers, plate heat exchangers (PHEs) are most widely used in small-scale ORC plants due to their high efficiency, compactness, disassembly flexibility, low cost, and requirement of low temperature difference [6,7]. To the best of the authors, the heat transfer correlations directly influence the design and performance prediction of the PHEs, which would certainly affect the working status of the whole ORC system. Hence the influence of different heat transfer correlations for predicting the performance of PHEs on the system is focused in this paper. However, the studies on the heat transfer correlations of plate heat exchangers have shown certain limitations so far no matter in prediction accuracy or number of correlations available for reference. It has been found that the accurately designed PHEs especially depend on the preciseness of two-phase heat transfer correlations of flow boiling and condensation, which contribute to calculating the heat transfer coefficient of the working fluid side [7–9]. However, as for the publicized two-phase heat transfer correlations for pure fluids, such as the Yan and Lin correlation [10], the Hsieh et al. correlation [7], etc., most of them are derived based on the experimental tests in which the working conditions do not prevail in the realistic application. For example, the flow boiling correlations are experimentally obtained at low temperatures while the evaporator of an ORC plant usually works at a much higher temperature level, which may result in a decrease in the credibility of the final calculation results for the evaporator and even the whole ORC system. To the best knowledge of the authors, only a few research works have studied the influence of heat transfer correlations on the heat exchanger, and only one relative article was found, which is reported by Lambert et al. [11]. It addresses how sensitive the total cost evaluation is to the uncertainties of the heat transfer correlations for shell and tube heat exchangers in three different test cases. There is no published research studying the influence of different two-phase heat transfer correlations on the performance of the heat exchanger and ORC system yet. Whether the correlations can be widely used for realistic working conditions in the evaporator and condenser of ORC and even for other types of working fluids has not been verified yet. Therefore, it is worth further studying the influence of different two-phase heat transfer correlations based on the different experimental data on the design of the heat exchangers in ORC.

On the other hand, many optimizations of the ORC system are conducted under certain design conditions. However, the thermodynamic parameters of low-grade heat energy resources utilized in the ORC system like the waste heat of industry and combustion engines are usually unstable [12–14] with the heat source temperature varying frequently. Thus, the operation conditions of the evaporator and condenser usually deviate from the design point. The heat exchanger's performance under off-design conditions greatly affects the ORC system [15]. Therefore, it is also indeed to research the off-design performance of the ORC system. For the same reason, the different heat exchangers designed by the different heat transfer correlations may also have a significant impact on the performance of the ORC system under the off-design conditions, which haven't been studied by any research yet.

To fill the research gap mentioned above, the main work carried out in this paper is divided into three aspects. Firstly, the simplified mathematic model of the ORC system is established and the optimal working fluid along with its operation status achieving the maximum net output power is screened by adjusting the evaporation and condensation

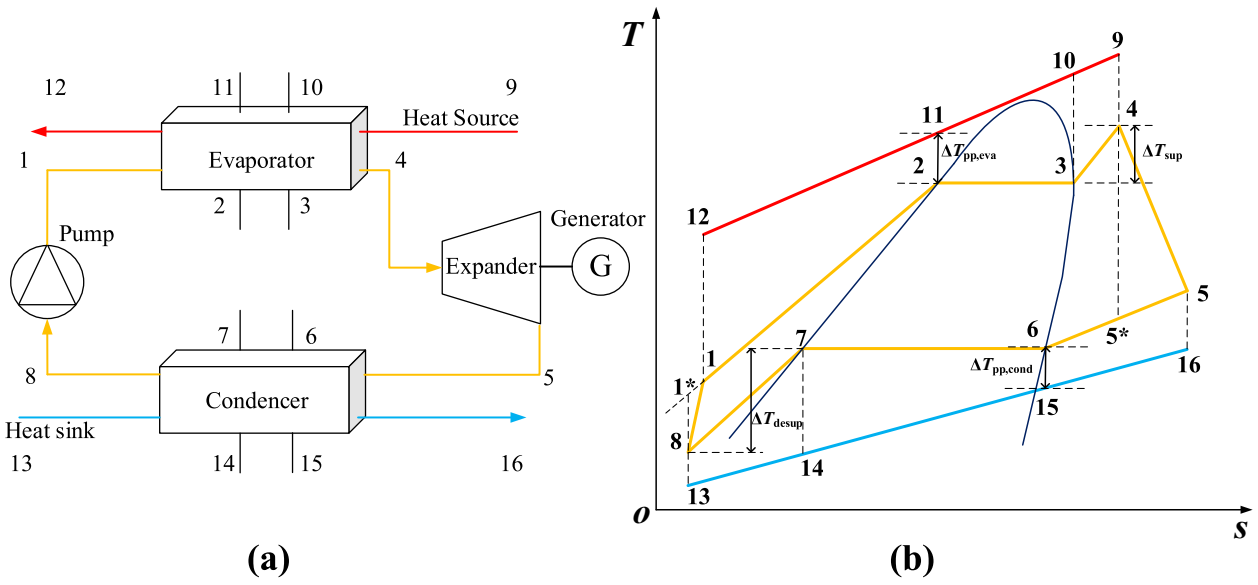

Fig. 1. (a) The simplified ORC system, (b) The T-s diagram of ORC.

Table 1
The initial input parameters of the ORC system.

Parameter	Symbol	Unit	Value
The inlet temperature of the heat source	$T_{hs,in}$	°C	140
The inlet temperature of the cold source	$T_{cs,in}$	°C	10
Pinch point of evaporation	$T_{pp,eva}$	°C	5
Pinch point of condensation	$T_{pp,cond}$	°C	5
Superheat degree	T_{sup}	°C	5
Subcooling degree	T_{cond}	°C	5
Isentropic efficiency of the pump	η_{pump}	–	0.8
Isentropic efficiency of the turbo	η_{turb}	–	0.8
Mass flow of heat source	m_{hs}	kg/s	7.5

pressures of 5 fluids. Secondly, four flow boiling correlations (Zhang et al. correlation [16], Yan and Lin correlation [10], Liu and Winterton correlation [17], and Amalfi et al. correlation [18]) and four flow condensation correlations (Zhang et al. correlation [19], Kuo et al. correlation [20], Han et al. correlation [21] and Yan et al. correlation [22]) are utilized to design the plate type evaporators and condensers based on the optimal working fluid as well as the operation condition screened. Comparison of the design size, economic and environmental performances among the heat exchangers is carried out. Thirdly, the influence of correlations used for the design of ORC heat exchangers under the design working condition on the ORC off-design performance is investigated. Comparative analysis of thermodynamic, economic, and environmental performances among different ORC systems which are distinguished by PHEs designed through various correlations is carried out. The results could provide guidelines for the heat transfer correlation selection to design PHEs preliminarily and evaluate the off-design performance of ORC systems.

2. Methods

2.1. The thermodynamic optimization model of ORC

2.1.1. The simplified ORC model

Based on the actual operating condition of a small-scale geothermal power plant [23], an ORC system with a capacity of around 0.3 MW net output power is focused and investigated in this paper. The layout of the ORC system consisting of four components (evaporator, expander, condenser and pump) is shown in Fig. 1. (a) To further describe the inner thermodynamic principle, the T-s diagram of the ORC cycle is displayed in Fig. 1. (b), and eight detailed processes are included intuitively. The continuous variation processes 1–4 happen in the evaporator cover preheating, evaporation, and superheating respectively. Similarly, processes 5–8 happening in the condenser consist of desuperheating, condensation, and subcooling respectively. All of the 6 processes above are assumed to be constant pressure processes. In processes 4–5, the superheated vapour expands and drives the expander through an adiabatic process. In process 8–1, the liquid working fluid is pumped adiabatically into the evaporator. The assumption of the cycle parameters is listed in Table 1.

Based on the description of the 8 processes in Fig. 1. (b), the thermodynamic model of the ORC system is illustrated as follows. The pinch point of the evaporator $T_{pp,eva}$ and the condenser $T_{pp,cond}$ can be defined as:

$$T_{pp,eva} = T_{hs,p} - T_{eva,in} \tag{1}$$

$$T_{pp,cond} = T_{cond,in} - T_{cs,p} \tag{2}$$

where $T_{hs,p}$, $T_{cs,p}$ are the temperature of the heat source and cold source at the pinch point, $T_{eva,in}$ and $T_{cond,in}$ are the temperature of working fluid at the inlet of the evaporator and condenser.

No pressure drop is assumed in the evaporator and the condenser:

$$p_{pump,out} = p_{eva,in} = p_{eva,out} = p_{turb,in} = p_{eva} \tag{3}$$

$$p_{turb,out} = p_{cond,in} = p_{cond,out} = p_{pump,in} = p_{cond} \tag{4}$$

where $p_{pump,in}$, $p_{pump,out}$, $p_{eva,in}$, $p_{eva,out}$, $p_{turb,in}$, $p_{turb,out}$, $p_{cond,in}$, $p_{cond,out}$ are the pressure of working fluid at the inlet and outlet of the pump, evaporator, expander, and condenser respectively.

The output power of the expander W_{turb} and the power consumption of the pump W_{pump} can be given individually as:

$$W_{turb} = m_f\left(h_{turb,in} - h_{turb,out}\right) \tag{5}$$

$$W_{pump} = m_f\left(h_{pump,out} - h_{pump,in}\right) \tag{6}$$

where $h_{turb,in}$, $h_{turb,out}$, $h_{pump,in}$, $h_{pumo,out}$ are the enthalpy of working fluid at the inlet and outlet of the expander and pump respectively, and m_f is the mass flow of the working fluid.

The isentropic efficiency of the expander η_{turb} and the pump η_{pump} are described as:

Table 2
The properties of working fluids [25–27].

Working fluid	Safety level	Fluid type	GWP	ODP	Critical pressure (bar)
R1234ze(E)	A2L	Dry	1	0	36.35
R245fa	B1	Dry	693	0	36.51
R236fa	A1	Dry	9810	0	32.00
R600a	A3	Dry	20	0	36.29
R1233zd(E)	A1	Dry	1	0	35.73

$$\eta_{turb} = \frac{h_{turb,in} - h_{turb,out}}{h_{turb,in} - h_{turb,out,is}} \tag{7}$$

$$\eta_{pump} = \frac{h_{pump,in,is} - h_{pump,out}}{h_{pump,in} - h_{pump,out}} \tag{8}$$

where $h_{turb,out,is}$ is the enthalpy of working fluid at the outlet of the expander through an ideal isentropic process, and $h_{pump,out,is}$ is the enthalpy of working fluid at the outlet of the pump assuming the pumping process is isentropic.

Based on the assumption of ignoring the heat loss, the heat transfer in the evaporator Q_{hs} and condenser Q_{cs} can be calculated respectively by:

$$Q_{hs} = m_{hs}\left(h_{hs,in} - h_{hs,out}\right) = m_f\left(h_{turb,in} - h_{pump,out}\right) \tag{9}$$

$$Q_{cs} = m_{cs}\left(h_{cs,in} - h_{cs,out}\right) = m_f\left(h_{turb,out} - h_{pump,in}\right) \tag{10}$$

where $h_{hs,in}$, $h_{hs,out}$, $h_{cs,in}$, $h_{cs,out}$ are the inlet and outlet temperature of the heat source and cold source respectively.

Therefore, the net output power and the thermal efficiency of ORC system W_{net} and η_I are defined as:

$$W_{net} = W_{turb} - W_{pump} \tag{11}$$

$$\eta_I = \frac{W_{net}}{Q_{hs}} \tag{12}$$

To evaluate the irreversible loss of the system, the exergy loss definitions of the components are illustrated below in order of evaporator I_{eva}, condenser I_{cond}, expander I_{turb} and pump I_{pump}:

$$I_{eva} = m_f T_{amb}\left[\left(s_{turb,in} - s_{pump,out}\right) - \frac{h_{turb,in} - h_{pump,out}}{T_{hs,mean}}\right] \tag{13}$$

$$I_{cond} = m_f T_{amb}\left[\left(s_{pump,in} - s_{turb,out}\right) - \frac{h_{pump,in} - h_{turb,out}}{T_{cs,mean}}\right] \tag{14}$$

$$I_{turb} = m_f\left(s_{turb,out} - s_{turb,in}\right) \tag{15}$$

$$I_{pump} = m_f\left(s_{pump,out} - s_{pump,in}\right) \tag{16}$$

where $s_{turb,in}$, $s_{turb,out}$, $s_{pump,in}$, $s_{pump,out}$ are the entropy of working fluid at the inlet and outlet of expander and pump respectively, and $T_{hs,mean}$, $T_{cs,mean}$ are the average temperatures of heat source and cold source.

The total exergy loss and the efficiency of the second thermodynamic law of the system I_{total} and η_{II} is given as:

$$I_{total} = I_{eva} + I_{cond} + I_{pump} + I_{turb} = m_f T_{amb}\left(\frac{h_1 - h_4}{T_{hs,mean}} - \frac{h_8 - h_5}{T_{cs,mean}}\right) \tag{17}$$

$$\eta_{II} = \frac{W_{net}}{Q_{hot}\left(1 - \frac{T_{cs,mean}}{T_{hs,mean}}\right)} \tag{18}$$

where T_{amb} is the ambient temperature.

2.1.2. Working fluid screening optimization model

Based on the thermodynamic model of ORC established above, the whole thermodynamic process then can be calculated and analyzed once the working fluid type is defined specifically. It is obvious that under a fixed thermal boundary condition, an optimal working fluid exists to achieve the highest net output power. Hence the working fluid screening optimization model is proposed to achieve the highest net output power. After the comprehensive consideration of the environmental protection aspect, safety level, and other properties, five fluids listed in Table 2 are selected as the working fluid candidates including R1234ze(E), R245fa, R236fa, R600a, and R1233zd, which were widely applied in the existing literature due to their superior thermodynamic performance, stability and low cost [24].

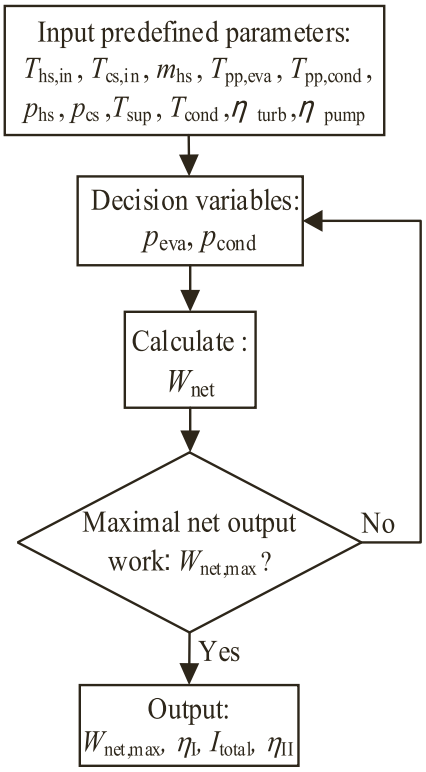

Fig. 2. The screening optimization flow of working fluids.

The working fluid screening optimization process is presented in Fig. 2. For each working fluid candidate, the evaporation and condensation pressures are chosen as decision variables. The maximum net output power is calculated for each working fluid composition, and the optimum working fluid is picked out among the results of considered candidates.

2.2. The design model of PHE

Given the optimum working fluid along with the corresponding working conditions above, the specific geometric size design programs of PHE then can be derived by adopting different heat transfer correlations. Due to the different experimental fluids and heat transfer

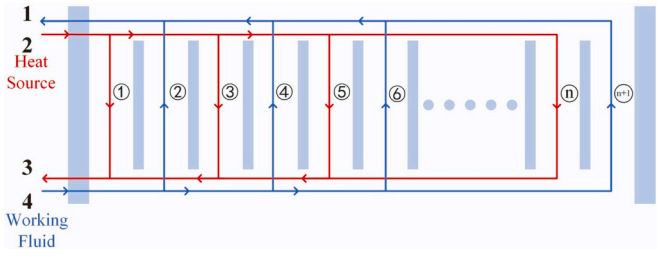

Fig. 3. Heat transfer process in PHE.

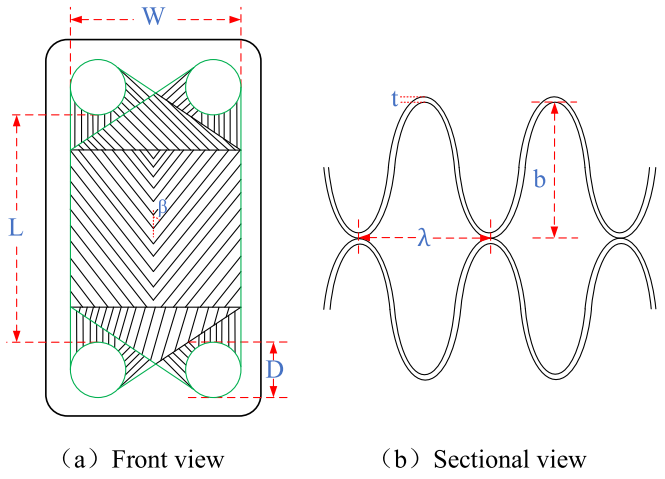

Fig. 4. Structure diagram of heat exchange plate (a) Front view, (b) Sectional view.

Table 3
Parameters of the chevron-corrugated plate.

Parameter	Symbol	Unit	Value
Width	w	m	0.5
Thickness	t	mm	0.5
Corrugation depth	b	mm	5
Corrugation wavelength	λ	mm	9
Chevron angle	β	°	60
Thermal conductivity	k	W/(m·K)	16.2

boundaries set in various references, there is a potential distinction among geometric size results of PHEs designed by different correlations. Further, this distinction may lead to a more obvious contrast under off-design working conditions, which is to be discussed emphatically in this paper. Here 4 flow boiling and 4 flow condensation correlations are selected for the two-phase heat transfer prediction in PHEs which are explained and illustrated in this part.

2.2.1. Geometric design parameters of the PHE

The PHE consists of numerous embossed or corrugated metal plates contacted with each other and the countercurrent flow process between the heat source and working fluids is exhibited in Fig. 3. The shape of the metal plate is an important character for the PHE. More than 60 types of plate patterns have been designed and the most widely-used and efficient pattern is the chevron corrugation shape offered by most manufacturers now [28].

There are usually two categories of geometric design parameters (corrugation shape and plate size) for the chevron corrugation plate as shown in Fig. 4. The geometric parameters of corrugation shape include the corrugation depth b, the chevron angle β, and the wavelength of surface corrugation λ. The diameter of port D, the effective plate width W and the length L belonging to the latter category are the relative parameters of plate size. The assumed parameters of PHE applied in this paper are shown in Table 3 and the remaining unknown parameters are designing parameters further derived according to the specific working conditions.

During the design process, to calculate the effective heat exchange area, the area-enlargement factor is defined as:

$$\varphi = \frac{1}{6}\left(1+\sqrt{1+X^2}+4\sqrt{1+\frac{X^2}{2}}\right) \tag{19}$$

where X is the dimensionless corrugation parameter:

Table 4
The experimental conditions of flow boiling correlations.

Correlation	Fluid type	Mass flux (kg/s·m^2)	T_{eva} (°C)	p_{eva} (bar)	Heat flux (kW/m^2)
Zhang et al. [16]	R1233zd(E) et al. (7 in total)	52 to 137	55 to 141	14.4 to 27.6	10 to 40
Amalfi et al. [18]	R410A et al. (13 in total)	8.5 to 100	−2 to 31	–	0.14 to 41.1
Yan and Lin [10]	R134a	55 to 70	25.5 to 31	6.75 to 8	11 to 15
Liu and Winterton [17]	Water et al. (5 in total)	12.4 to 8179	0.2 to 62.3	8 to 197.5	0.35 to 2620

$$X = \frac{b\pi}{\lambda} \tag{20}$$

2.2.2. Flow boiling correlations of the two-phase region

The selection of heat transfer correlation is the most critical aspect of designing PHEs. Four correlations are selected and compared to predict the heat transfer coefficient of evaporation in the PHEs and they are Zhang et al. correlation [16], Yan and Lin correlation [10], Liu and Winterton correlation [17] and Amalfi et al. correlation [18]. All of them are empirical correlations derived from the experimental data and the experimental conditions for each correlation are summarized in Table 4.

The correlation proposed by Zhang et al. [16] was derived from the superposition model in the study of Chen et al. [29], which split the flow boiling coefficient into a linear superposition of nucleate boiling heat transfer coefficient and convective boiling heat transfer coefficient. In this study, the correlation suggested by Cooper [30] and Dittus-Boelter [31] was adopted to estimate the nucleate boiling heat transfer coefficient and convective boiling heat transfer coefficient of the PHEs respectively. It is worth noting that, empirical correlations are usually obtained by fitting the experimental data at a relatively low-temperature level, but the correlation proposed by Zhang et al. [16] is directly obtained by a linear combination of former correlations which are more suitable for higher temperature working conditions. Since the working condition of the PHEs in the ORC system was at a relatively high-temperature level, it is believed that the correlation proposed by Zhang et al. [16] may be more proper for the designing of PHEs in the ORC system. The mathematical expression of the Zhang et al. correlation [16] is defined as follows:

$$\alpha_{tp} = S\alpha_{pool} + F\alpha_l \tag{21}$$

$$F = 2.35\left(X_{tt}^{-1}+0.213\right)^{0.736} \tag{22}$$

$$S = \left[1+2.53\cdot10^{-6}\left(Re_l F^{1.25}\right)^{1.17}\right]^{-1} \tag{23}$$

$$X_{tt} = \left(\frac{\rho_v}{\rho_l}\right)^{0.5}\left(\frac{\mu_l}{\mu_v}\right)^{0.1}\left(\frac{1-x}{x}\right)^{0.9} \tag{24}$$

$$\alpha_{pool} = 35P_r^{0.12}\left(-log_{10}P_r\right)^{-0.55}M^{-0.5}q^{0.67} \tag{25}$$

$$\alpha_l = 0.023Re_l^{0.8}Pr_l^{0.4}\frac{k_l}{d_h} \tag{26}$$

where α_{tp} is the flow boiling heat transfer coefficient of the working fluid, α_{pool} is the nucleate boiling heat transfer coefficient calculated by Cooper et al. correlation [32], α_l is the single-phase heat transfer coefficient of working fluid calculated by Dittus-Boelter et al. correlation [31], S is the suppression factor, F is the enhancement factor, Re_l and Re_v are the liquid and vapour Reynolds number.

Through dimensional analysis and multiple regression analysis, the

Table 5
The experimental conditions of flow condensation correlations.

Correlation	Fluid	Mass flux (kg/s·m^2)	T_{cond} (°C)	p_{cond} (bar)	Heat flux (kW/m^2)
Zhang et al. [19]	R1234ze (E) et al.	16–90	29.7–71	2.9–16.3	4–57.4
Yan et al. [22]	R134a	60–120	26.7	7–9	10–16
Kuo et al. [20]	R410A	50–150	–	14.4–19.5	10–20
Han et al. [21]	R22 and R410A	13–34	20–30	–	4.7–5.3

correlation proposed by Amalfi et al. [18] was developed based on a huge experimental database including 1903 heat transfer test results of the PHE. Compared with the correlations proposed by Danilova et al. [33], Han et al. [21], Huang et al. [34], Donowski and Kandlikar et al. [35], and Hsieh and Lin et al. [7], the one of Amalfi et al. [18] supported by a more sufficient experimental database can be more accurate to predict the Nusselt number, which is defined as follows:

$$\begin{aligned} Nu_{tp} &= 982\cdot\beta^{*1.01}We_m^{0.315}Bo^{0.32}\rho^{*-0.224}, \text{When } Bd<4. \\ Nu_{tp} &= 18.495\cdot\beta^{*0.248}Re_v^{0.135}Re_{lo}^{0.351}Bd^{0.235}Bo^{0.198}\rho^{*-0.223}, \text{When } Bd\geq 4. \end{aligned} \tag{27}$$

where ρ^* is the density ratio, Nu_{tp} is the Nussel number of the working fluid in a two-phase region, β is the reduced chevron angle, We_m is the homogeneous Weber number, and Re_{lo} is the liquid-only Reynolds number.

The Yan and Lin correlation [10] is a typical mothed developed for predicting the heat transfer coefficient, which is proposed via R-134a in a transparent and visible PHE. Due to its simplicity and accuracy, it has been widely used for the flow boiling calculation of PHEs in numerous studies [36,37]. The Yan and Lin correlation [10] is defined as follows:

$$Nu_{tp} = \frac{d_h\alpha_{tp}}{\lambda_l} = 1.926Pr_l^{1/3}Bo_{eq}^{0.3}Re_{eq}^{0.5}\left[1-x_m+x_m\left(\frac{\rho_v}{\rho_l}\right)^{0.5}\right] \tag{28}$$

where Pr_l is the liquid Prandtl number, Re_{eq} is the equivalent of all liquid Reynolds, Bo_{eq} is the equivalent of all boiling numbers, and x_m is the average vapour quality between the inlet and exit.

The heat transfer process in the tubes and PHEs are similar to each other in many aspects, which leads to the application of the tube flow boiling correlations in PHEs [38]. Some studies utilized tube correlations to predict the heat transfer coefficient in PHEs while designing [39,40]. The tube correlation proposed by Liu and Winterton derived from the research of Kutateladze [41] in which an abundant database containing 4202 saturated boiling data points and 991 subcooled boiling data points in tubes was used. The Liu and Winterton correlation [17] is defined as follows:

$$\alpha_{tp} = \sqrt{\left(S\alpha_{pool}\right)^2+\left(F\alpha_l\right)^2} \tag{29}$$

$$\alpha_l = 0.023\left(\frac{k_l}{d_h}\right)Re_l^{0.8}Pr_l^{0.4} \tag{30}$$

$$\alpha_{pool} = 55P_r^{0.12}\left(-lgP_r\right)^{-0.55}M^{-0.5}q^{0.67} \tag{31}$$

$$F = \left[1+xPr_l\left(\frac{\rho_l}{\rho_v}-1\right)\right]^{0.35} \tag{32}$$

$$S = \frac{1}{1+0.55F^{0.1}Re_l^{0.16}} \tag{33}$$

where α_{pool} is the pool boiling heat transfer coefficient calculated by Cooper et al. correlation [32].

2.2.3. Condensation correlations of the two-phase region

For the condensation process, four semi-empirical correlations are also implemented to estimate the heat transfer coefficient of the PHE: the Zhang et al. correlation [19], the Kuo et al. correlation [20], the Han et al. correlation [21] and the Yan et al. correlation [22]. The working condition for each correlation is summarized in Table 5.

The Zhang et al. correlation [19] is suitable to predict the heat transfer coefficient of the plate condenser for both ORC systems and heat pump units. This correlation mainly considers the situation when the channel size is very narrow such as 1– 5 mm and even smaller. As the heat transfer coefficient is affected by the surface tension significantly, this correlation considers the surface tension, which has never been discussed in other existing correlations concerning condensation in PHEs. The Zhang et al. correlation [19] is defined as follows:

$$Nu_{tp} = 4.3375\cdot Re_{eq}^{0.5383}Pr_l^{1/3}Bo_1^{-0.3872} \tag{34}$$

$$Bo_l = \frac{g(\rho_l-\rho_v)D_h^2}{\sigma} \tag{35}$$

where Bo_1 is the boiling number defined in the Zhang et al. correlation [19].

The Kuo et al. correlation [20] is modified from the Kandlikar et al. correlation [42] and derived via the working fluid of R-410A with a corrugated sinusoidal shape of a chevron angle of 60°. According to the variations of the measured condensation heat transfer coefficient with the mean vapour quality in the experiment, the condensation heat transfer coefficient equation is fitted. The Kuo et al. correlation [20] is defined as follows:

$$\alpha_{tp} = \alpha_{r,l}\left[0.25Co^{-0.45}Fr_l^{0.25}+75Bo_2^{0.75}\right] \tag{36}$$

$$\alpha_{r,l} = 0.2092\left(\frac{k_l}{d_h}\right)Re_l^{0.78}Pr_l^{1/3}\left(\frac{\mu_{ave}}{\mu_{wall}}\right)^{0.14} \tag{37}$$

$$Co = \left(\frac{\rho_v}{\rho_l}\right)\left[\frac{(1-x_m)}{x_m}\right]^{0.8} \tag{38}$$

$$Fr_l = \frac{G^2}{\rho_l^2 g d_h} \tag{39}$$

$$Bo_2 = \frac{q}{Gh_{fg}} \tag{40}$$

where Bo_2 is the boiling number defined in the Kuo et al. correlation [20], $\alpha_{r,1}$ is the convective boiling heat transfer coefficient, h_{fg} is the difference of enthalpy for working fluid between the liquid phase and vapour phase, Fr_l is the liquid Froude number, Co is the convection number, μ_{ave} is the dynamic viscosity at the average temperature, μ_{wall} is the dynamic viscosity at the wall temperature.

The Han et al. correlation [21] is derived via research on the condensation processes of R-410A in three brazed PHE with chevron angles of 20, 35, and 45°. It is found that the geometric parameters especially the chevron angle must be taken into account in the correlation, which is defined as follows:

$$Nu_{tp} = Ge_1Re_{eq}^{Ge_2}Pr^{1/3} \tag{41}$$

$$Ge_1 = 11.22\left(\frac{\lambda}{d_h}\right)^{-2.83}\left(\frac{\pi}{2}-\beta\right)^{-4.5} \tag{42}$$

$$Ge_2 = 0.35\left(\frac{\lambda}{d_h}\right)^{0.23}\left(\frac{\pi}{2}-\beta\right)^{1.48} \tag{43}$$

where Ge_1 and Ge_2 are the non-dimensional geometric parameters that involve the corrugation pitch, the equivalent diameter, and the chevron angle.

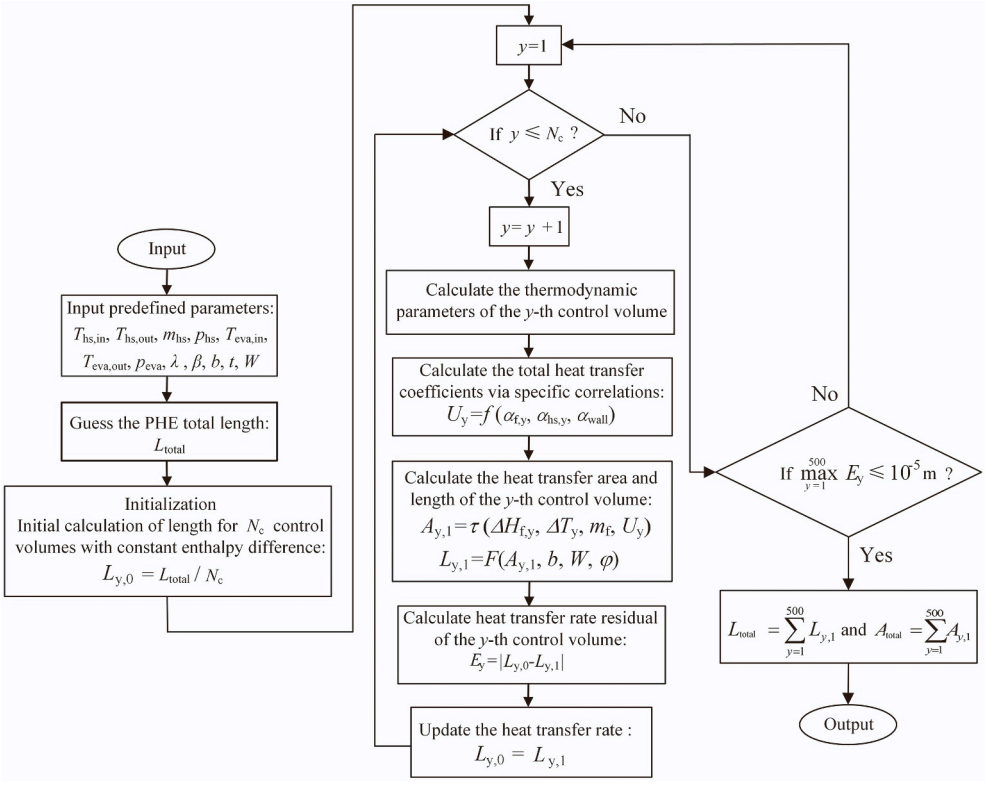

Fig. 5. The design workflow of the evaporator.

The Yan et al. correlation [22] is a classic flow condensation correlation widely used by many studies [43,44]. This correlation is proposed to predict the heat transfer coefficient of R-134a in PHEs and the experiment data for fitting the correlations contain the mass flux of R-134a, average imposed heat flux, system pressure, and vapour quality. The Yan et al. correlation [22] is defined as follows:

$$Nu_{tp} = 4.118 Re_{eq}^{0.4} Pr_l^{1/3} \tag{44}$$

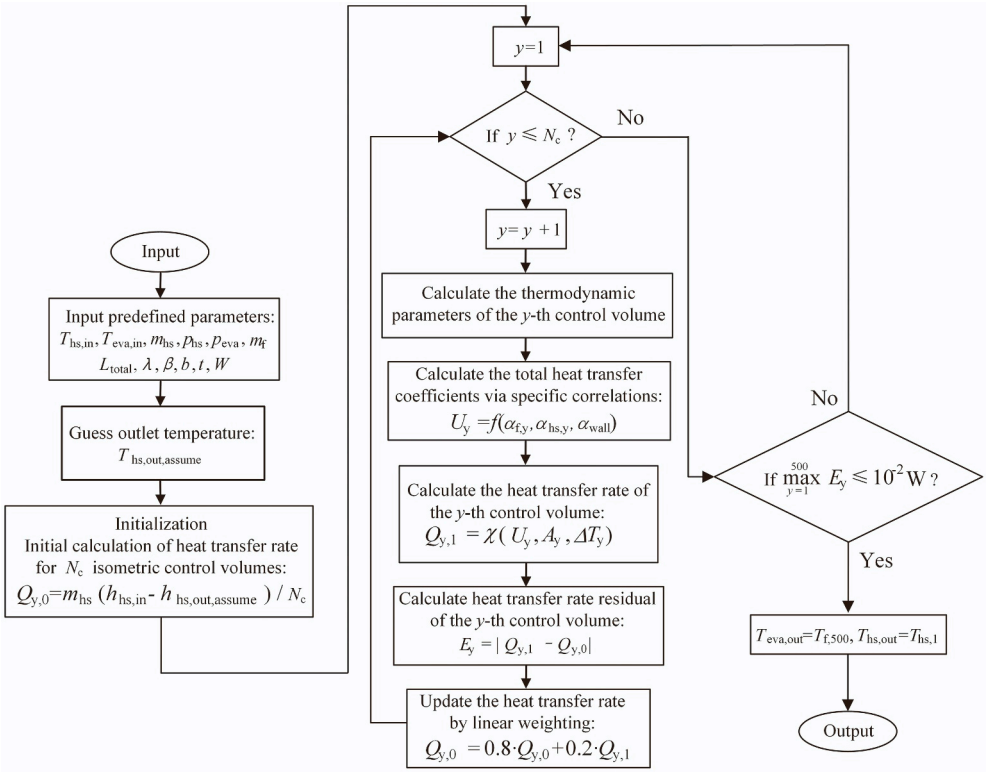

Fig. 6. The rating process of the evaporator.

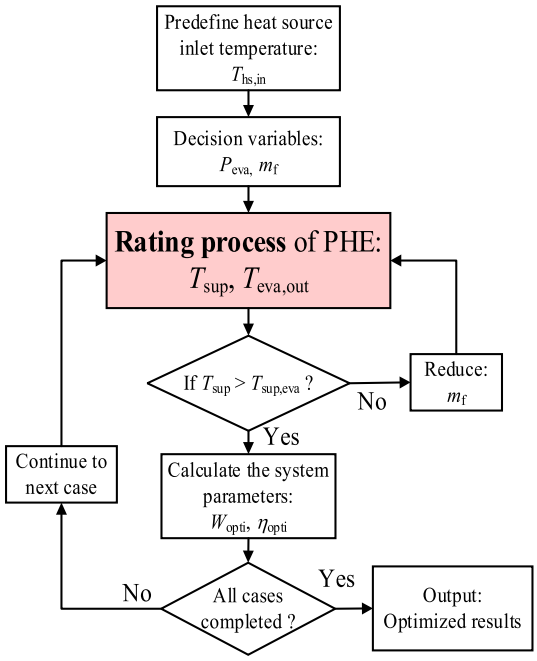

Fig. 7. The optimization workflow under off-design conditions.

2.2.4. Correlation of single-phase region

In this paper, the single-phase heat transfer of liquid or gas region in PHE is predicted through a commonly used correlation by Martin in 1996 [45], which is given by:

$$Nu_{sp} = 0.122Pr^{1/3}\left(\frac{\mu_{ave}}{\mu_{wall}}\right)^{1/6}\left(fRe^2 sin2\beta\right)^{0.374} \quad (45)$$

where Nu_{sp} is the Nussel number in the single-phase region and the correction coefficient f is given as follows,

$$\frac{1}{f^{0.5}} = \frac{cos\beta}{(0.18tan\beta + 0.36sin\beta + f_0/cos\beta)^{0.5}} + \frac{(1-cos\beta)}{(3.8f_1)^{0.5}} \quad (46)$$

when $Re < 2000, f_0 = \frac{64}{Re}$, $f_1 = \frac{579}{Re} + 3.85$when $Re \geq 2000, f_0 = (1.811gRe - 1.5)^{-2}$.$f_1 = \frac{39}{Re^{0.289}}$.

2.2.5. Design workflow of PHEs

Taking the evaporator as an example, the workflow of the PHE design code is shown in Fig. 5. The input thermodynamic parameters are calculated in the simplified ORC model and the predefined geometric parameters are shown in Table 3. By dividing the heat transfer channel into numerous control volumes in the length direction, the steady-state energy, mass, and momentum conservation equations were solved in each control volume. The more control volumes divided, the more accurate the calculation results would be, but the higher the calculation cost of the program would be. Therefore, in this study, the total number of 500 control volumes were selected after a trade-off between the precision and the cost of the calculation time. For each control volume, the length calculation residual is set as 10^{-5} m.

2.3. The off-design performance evaluation model of the ORC system

2.3.1. The detailed ORC model considering the designed geometric size of PHEs

Adoption of various correlations under designed working conditions more or less leads to the difference of geometric size parameters among the designed PHEs, which may further have an impact on the performance of ORC under off-design working conditions. To investigate the effect of the different correlations on the off-design performance of the ORC system, the designed geometric size parameters of PHEs are considered and embedded into the detailed ORC model. In other words, once the detailed geometric size parameters of PHEs are considered specifically in the ORC simulation model, the heat transfer process in the PHEs will be simulated in detail rather than derived briefly according to the given assumptions such as superheat (subcooling) and evaporation (condensation) temperatures in the simplified ORC model. Taking the evaporator as an example, the detailed PHE simulation process is realized through the rating process of the PHE presented in Fig. 6. The finite volume method is adopted and the number of control volumes N_c of each PHE is set to 500 in this paper. The heat transfer residual of each PHE is defined as 10^{-2} W to achieve a high calculation precision. For the other two processes (4–5 of expander and 8–1 of pump shown as Fig. 1) in the detailed ORC model, the simulation assumption keeps no change. In this way, the detailed ORC model involving the designed geometric size of PHEs is established.

Table 6
The results of working fluid screening.

Fluid	p_{eva} (bar)	p_{cond} (bar)	W_{net} (kW)	η_I	η_{II}	I_{total} (kW)
R1234ze (E)	29	5.2	307.6	11.00%	50.90%	304.9
R236fa	16	2.7	289.2	10.75%	48.74%	312.8
R600a	16.7	3.4	278.6	11.20%	49.03	298.4
R245fa	11.0	1.4	267.9	11.90%	50.21%	273.9
R1233zd (E)	10.7	1.2	246.4	13.20%	52.51%	230.6

2.3.2. The off-design performance evaluation model

Based on the detailed ORC model, the optimization of the system net output power under different off-design conditions is carried out as displayed in Fig. 7. The off-design conditions are arranged mainly by the temperature variation of the heat source which is set from 120 °C to 160 °C with an increment of 5 °C, while the mass flow of the heat source remains unchanged. The net output power chosen as the optimization target is maximized under each considered off-design condition. The evaporation pressure and mass flow of working fluid are set as the decision variables. Notably, the step marked in red in Fig. 7 is a brief expression of the rating process claimed in Fig. 6. And the off-design conditions are arranged as follows: for each heat source inlet temperature, the decision variables are defined under 9 different reduced pressures. The variation of the reduced pressure of evaporation ranges from 0.32 to 0.96 with equal intervals [46–48] in this paper. Hence the complete strategy and workflow for the ORC system optimization is proposed as shown in Fig. 7.

Through the optimization process, the maximum thermodynamic performance parameters under off-design conditions are screened. However, in reality, other system performances such as economic and environmental performances are usually considered in the evaluation works [49,50]. To investigate the system economic and environmental performance differences among different cycles characterized through different correlations under off-design conditions, relative indicators of *EPC* (electricity production cost)and *GHG* (greenhouse gas emission) are utilized respectively in this paper [51,52]. Detailed definitions and calculations of these indicators are provided in Appendix A and Appendix B.

3. Results and discussion

3.1. Working fluid screening optimization

The maximized net output power of each working fluid along with other thermodynamic performance parameters is listed in Table 6 and

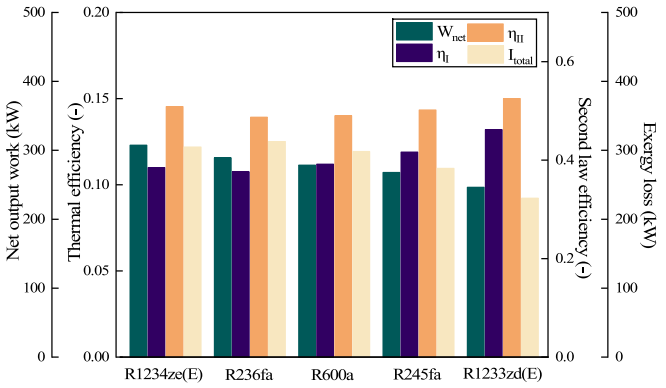

Fig. 8. Comparison for working fluid screening.

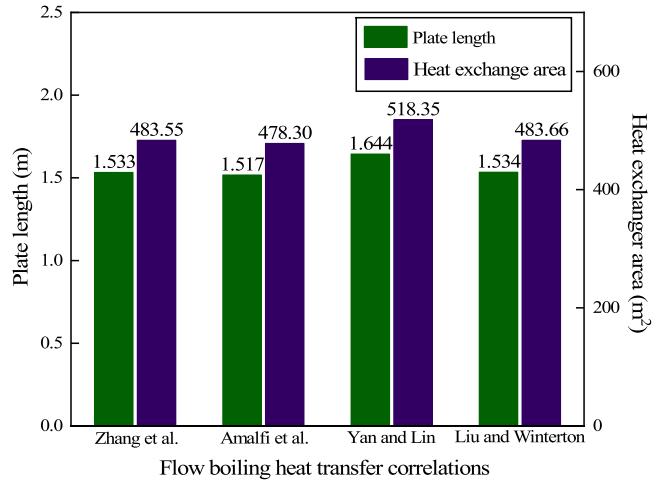

Fig. 9. Design results of evaporators.

shown in Fig. 8. It can be seen that R1234ze(E) is competent to get the maximum net output power and a high thermodynamic second efficiency at the evaporation pressure of 29 bar and the condensation pressure of 5.2 bar even though the second largest exergy loss is obtained. Moreover, R1233zd(E) can achieve the maximum thermal efficiency, the maximum thermodynamic second efficiency, and the minimum exergy loss at the evaporation pressure of 10.7 bar and the condensation pressure of 1.2 bar whereas the net output power is the minimum. As for the remaining 3 fluids, the ORC system performance parameters behave worse than that of R1234ze(E) and R1233zd(E). For instance, the highest η_I and η_{II} as well as minimum I_{total} is obtained by R1233zd(E). Also, the highest W_{net} is gained by R1234ze(E). The fluid R245fa widely utilized in many studies achieves an appreciable thermal efficiency but a worse net output power, while R236fa and R600a realize a relatively higher net output power but an unsatisfactory thermal efficiency.

Hence, it is hard to find a fluid with an all-around performance from the 5 fluids above. To maximize the net output work generated by the ORC system, the net output power is taken as the most significant evaluation parameter in this paper, thus the fluid R1234ze(E) was selected as the optimal fluid along with the working condition at which the evaporation pressure is 29 bar and the condensation pressure is 5.2 bar.

3.2. Design results of the plate heat exchanger

Based on the optimal working fluid R1234ze(E) along with the ORC working condition chosen as the design condition of PHEs, the plate

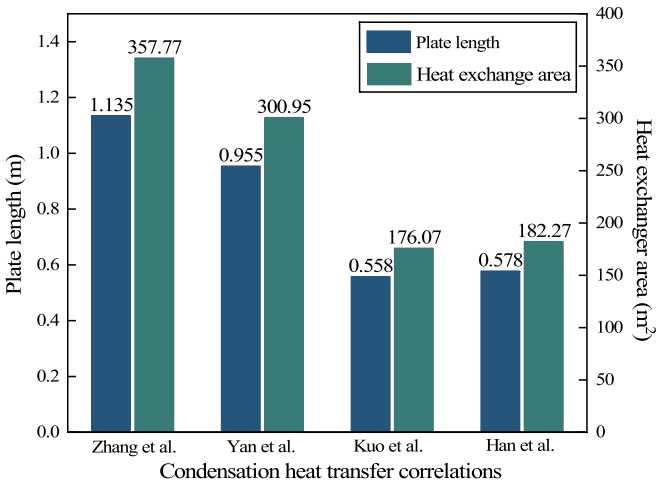

Fig. 10. Design results of condensers.

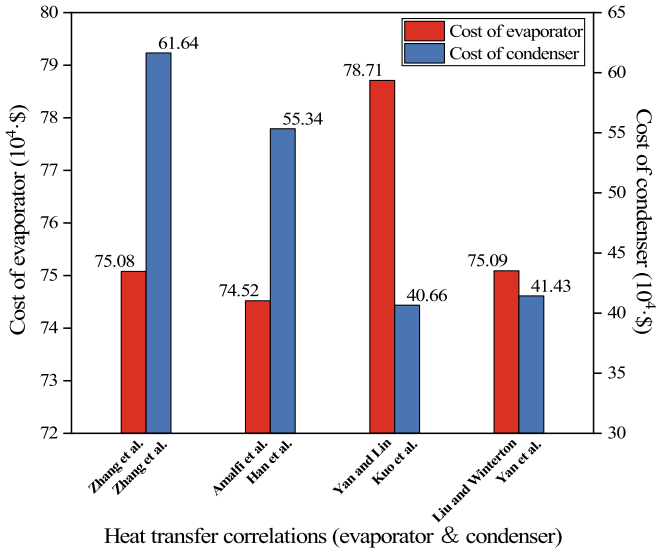

Fig. 11. Cost evaluation of PHEs.

length and the corresponding heat exchange area of the evaporators and condensers designed by four different flow boiling correlations and four different flow condensation correlations are shown in Fig. 9 and Fig. 10 respectively. The plate length of the evaporator estimated by the Yan and Lin correlation [10] is the maximum and 8.37% longer than the minimum one predicted by Amalfi et al. correlation [18]. As for the condenser, the maximum difference is almost 100% between the maximum plate length predicted by Zhang et al. correlation [19] and the minimum plate length estimated by the Kuo et al. correlation [20]. It's obvious that the variance of the designed length of the condenser is much larger than that of the evaporator, this is because whether in the evaporator or condenser, the same correlation is used to predict the single-phase heat transfer coefficient, which means the same calculated length of the single-phase section. In the evaporator, the single-phase preheating process accounts for most of the total length due to the large difference between the inlet temperature of the working fluid and the evaporation temperature. On the contrary, the outlet temperature of working fluids from the expander is close to the condensation temperature, so the main part of the condenser length is dominated by the two-phase condensation process which is predicted by different flow condensation correlations. Therefore the impact of different two-phase correlations on the PHE geometric size design depends on the actual

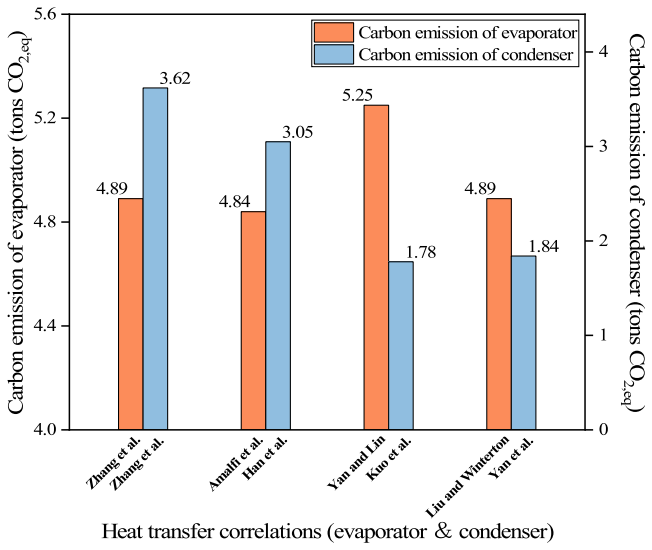

Fig. 12. Carbon emission evaluation of PHEs.

length of the two-phase heat transfer region in the PHE to a certain extent.

What's more, it is found that the evaporator geometry size designed by Zhang et al. correlation [16] is almost the same as that of Liu and Winterton correlation's [17]. This is probably because of their similar estimation method about the two-phase heat transfer coefficient by weighting the nucleate boiling heat transfer coefficient and convective boiling heat transfer coefficient derived from the correlations of Cooper [30,32] and Dittus-Boelter [31]. Similarly, the condenser size designed by Kuo et al. correlation [20] is close to the one designed by Han et al. correlation [21] because both of the correlations are derived from the fluid R410A.

To compare the impact of different correlations on the economic and environmental performances of designed PHEs, the heat exchangers' cost and carbon emission during manufacturing and recycling processes are calculated and shown in Fig. 11 and Fig. 12. The definition of the economic and environmental performance parameters is provided in the Appendix A and B. Since the cost of a heat exchanger is directly related to its heat transfer area, the cost change of condensers among different correlations is more obvious than that of evaporators and the largest cost variation is almost 210 thousand dollars which covers nearly half the cheapest condenser's expense. As for the carbon emission amount, manufacturing and recycling of materials used in PHEs consist the main

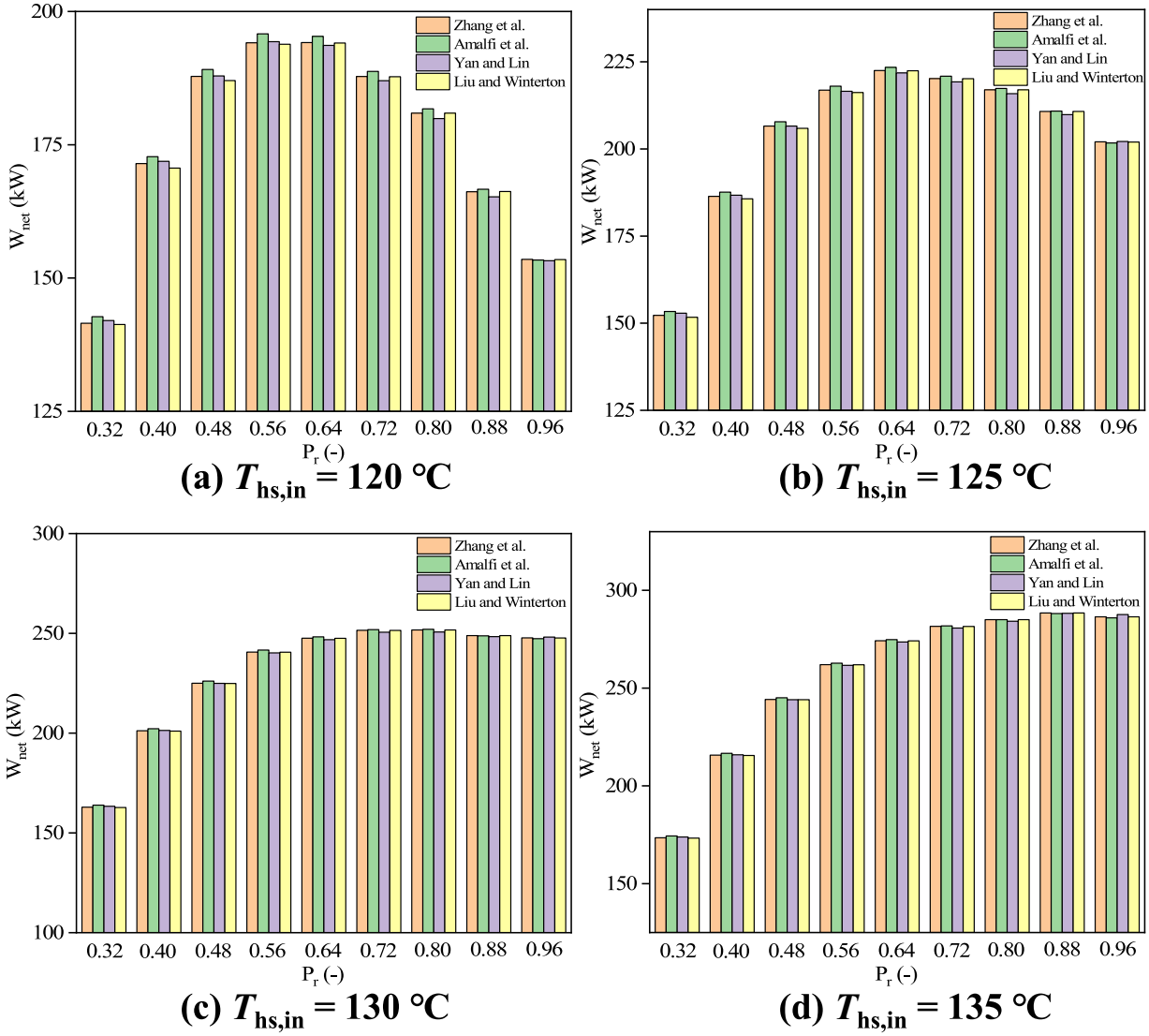

Fig. 13. Variation of W_{net} with P_r at $T_{hs,in}$ = (a) 120 °C, (b) 125 °C, (c) 130 °C, (d) 135 °C.

Table 7
Maximum results under different heat source temperatures.

$T_{hs,in}$ (°C)	Maximum W_{net} (kW)	Corresponding P_r (−)	Corresponding correlation
120	195.8	0.56	Amalfi et al. [18]
125	223.4	0.64	Amalfi et al. [18]
130	252.0	0.80	Amalfi et al. [18]
135	288.5	0.88	Liu and Winterton [17]
145	360.0	0.96	Yan and Lin [10]
150	392.9	0.96	Yan and Lin [10]
155	423.5	0.96	Yan and Lin [10]
160	451.7	0.96	Yan and Lin [10]

part. Hence a similar difference is presented in Fig. 12 and the more apparent distinction of carbon emission among condensers is found. The highest carbon emission among the condensers is almost twice as much as the lowest. Therefore, the selection of correlations can significantly influence the final evaluation index which may cause an unforeseeable uncertainty during the heat exchanger's design and performance evaluation processes.

3.3. Comparative analysis of ORC performance under off-design conditions

From the perspective of component, design size, economic and environmental performance parameters of PHEs designed by various heat transfer correlations are compared preliminarily and noticeable differences are analyzed. To further discuss the impact of different correlations on the performance evaluation of the whole ORC system, off-design condition analysis is conducted by changing the heat source inlet temperature. To simulate the change of heat source, the inlet temperature varies from 120 °C to 160 °C and the mass flow remains to be constant at 7.5 kg/s. The net output power is the optimization objective and the decision variables are the mass flow of working fluid and the evaporation pressure. Then the variation of performance of the ORC system under different off-design conditions and different heat exchangers designed from 8 correlations will be compared and analyzed in this part.

Different behaviours among the PHEs would affect the operating conditions of other components in the ORC system, which would certainly lead to an obvious variation of the off-design operation conditions of the whole system. To investigate the system's off-design performance with a proper consideration of this influence in this paper the inlet status of the evaporators is fixed. In this way, all the PHEs would be operated under a similar off-design condition and the comparative analysis among different correlations would be conducted under an ideal unified boundary.

3.3.1. Comparative analysis of thermodynamic performance

In the off-design simulation process, the outlet status of the evaporator determines the net output power under the unified boundary condition. In other words, the net output power is associated with the flow boiling correlations used to predict the performance of evaporators. The variation characteristics of the net output power with reduced pressure P_r under different heat source temperatures as well as various flow boiling correlations are visually displayed in Fig. 13 partly and all the maximum results are listed in Table 7. The reason why the variation characteristics under only 4 heat source temperatures are discussed is that the single-peak pattern disappears under the other 4 heat source boundaries. To discuss the single-peak phenomenon particularly, deeper discussion is conducted in this paper. It is obvious that under a certain heat source and a specific reduced pressure, the difference of W_{net} among different flow boiling correlations seems to be not significant, which has been shown clearly in Fig. 13. Also, as for the maximum results listed in Table 7 the change of corresponding correlations is not very obvious and shows nearly no regular characteristic. To further present this indistinct difference, the relative difference of the maximum W_{net} calculated by different correlations is listed in Table 8. It can be seen that the relative difference is tiny and ranges from 0.49% to 1.10%.

Table 8
Relative difference of the maximum W_{net} calculated by different correlations.

$T_{hs,in}$ (°C)	Highest maximum W_{net} (kW)	Lowest maximum W_{net} (kW)	Relative difference
120	195.8 kW (Amalfi et al. [18])	193.8 kW (Liu and Winterton [17])	1.03%
125	223.4 kW (Amalfi et al. [18])	221.8 kW (Yan and Lin [10])	0.72%
130	252.0 kW (Amalfi et al. [18])	250.6 kW (Yan and Lin [10])	0.56%
135	288.5 kW (Liu and Winterton [17])	287.1 kW (Amalfi et al. [18])	0.49%
145	360.0 kW (Yan and Lin [10])	357.0 kW (Amalfi et al. [18])	0.84%
150	392.9 kW (Yan and Lin [10])	388.8 kW (Amalfi et al. [18])	1.05%
155	423.5 kW (Yan and Lin [10])	419.0 kW (Amalfi et al. [18])	1.07%
160	451.7 kW (Yan and Lin [10])	446.8 kW (Amalfi et al. [18])	1.10%

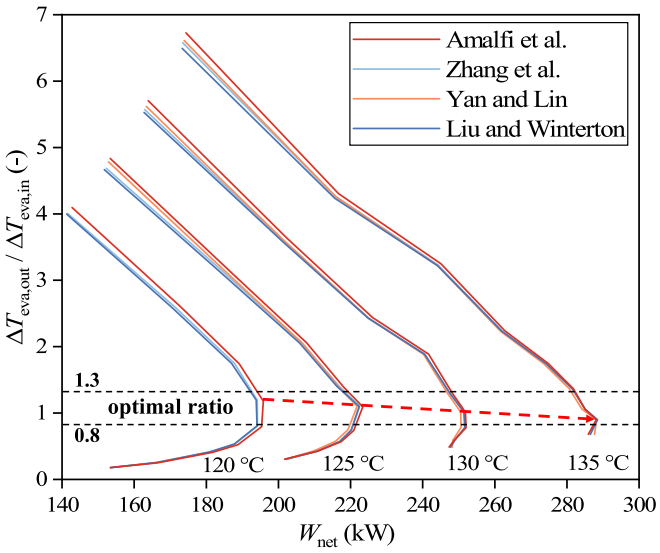

Fig. 14. Variation of the ratio ($\Delta T_{eva,out}/\Delta T_{eva,in}$) with the W_{net}.

However, the maximum W_{net} varies apparently under different heat source temperatures as listed in Table 7. With the increase of $T_{hs,in}$ from 120 °C to 160 °C, the maximum W_{net} rises from 195.8 kW to 451.7 kW. At the same time, the corresponding P_r values under different maximum W_{net} values vary with the $T_{hs,in}$. It can be seen that the corresponding P_r value increases gradually while $T_{hs,in}$ increases from 120 °C to 135 °C but remains to be constant while $T_{hs,in}$ increases from 145 °C to 160 °C. This is due to the limitation of working fluid properties that cannot be suitable for the utilization of higher heat source temperatures. To explain the increase of the corresponding P_r value while $T_{hs,in}$ increases from 120 °C to 135 °C, the temperature distribution characteristic of the evaporator is discussed. The variation of the ratio of temperature difference (between the heat source and working fluid) at the outlet and that at the inlet with the $T_{hs,in}$ is presented in Fig. 14.

It's clear that there is existing an optimum reduced pressure achieving the maximum W_{net} under each off-design condition from Fig. 13. And the increasing trend of P_r can be found in Table 7 as the $T_{hs,in}$ increases from 120 °C to 135 °C. To particularly explain this trend, the variation of the ratio ($\Delta T_{eva,out}/\Delta T_{eva,in}$) with the W_{net} under each $T_{hs,in}$ is presented in Fig. 14.

As shown in Fig. 14, it can be found that the shape of the curves is analogous parabola like and the optimal ratio ($\Delta T_{eva,out}/\Delta T_{eva,in}$) ranges from 0.8 to 1.3. This means an appropriate match for the temperature level of the heat source and the working status of the fluid should be

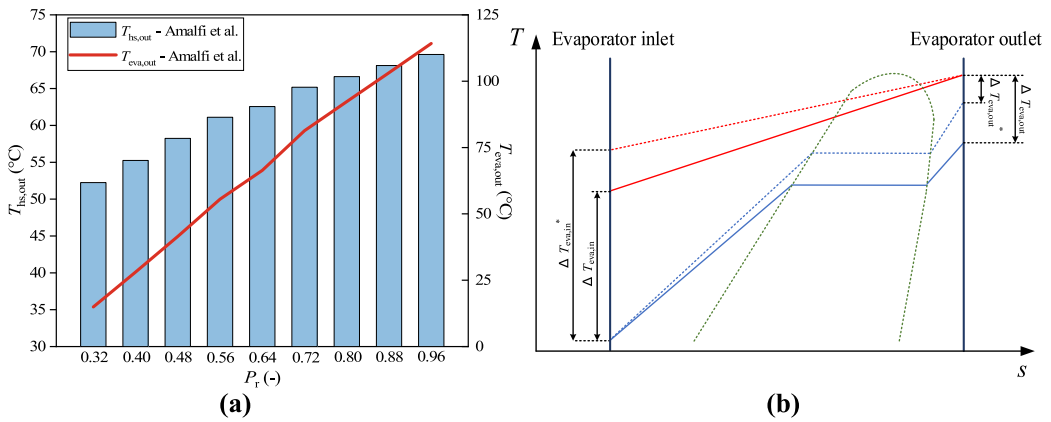

Fig. 15. (a) Variation of $T_{hs,out}$ and $T_{eva,out}$ at $T_{hs,in}$ = 125 °C; (b) Variation of $\Delta T_{eva,out}$ and $\Delta T_{eva,in}$ with reduced pressure P_r.

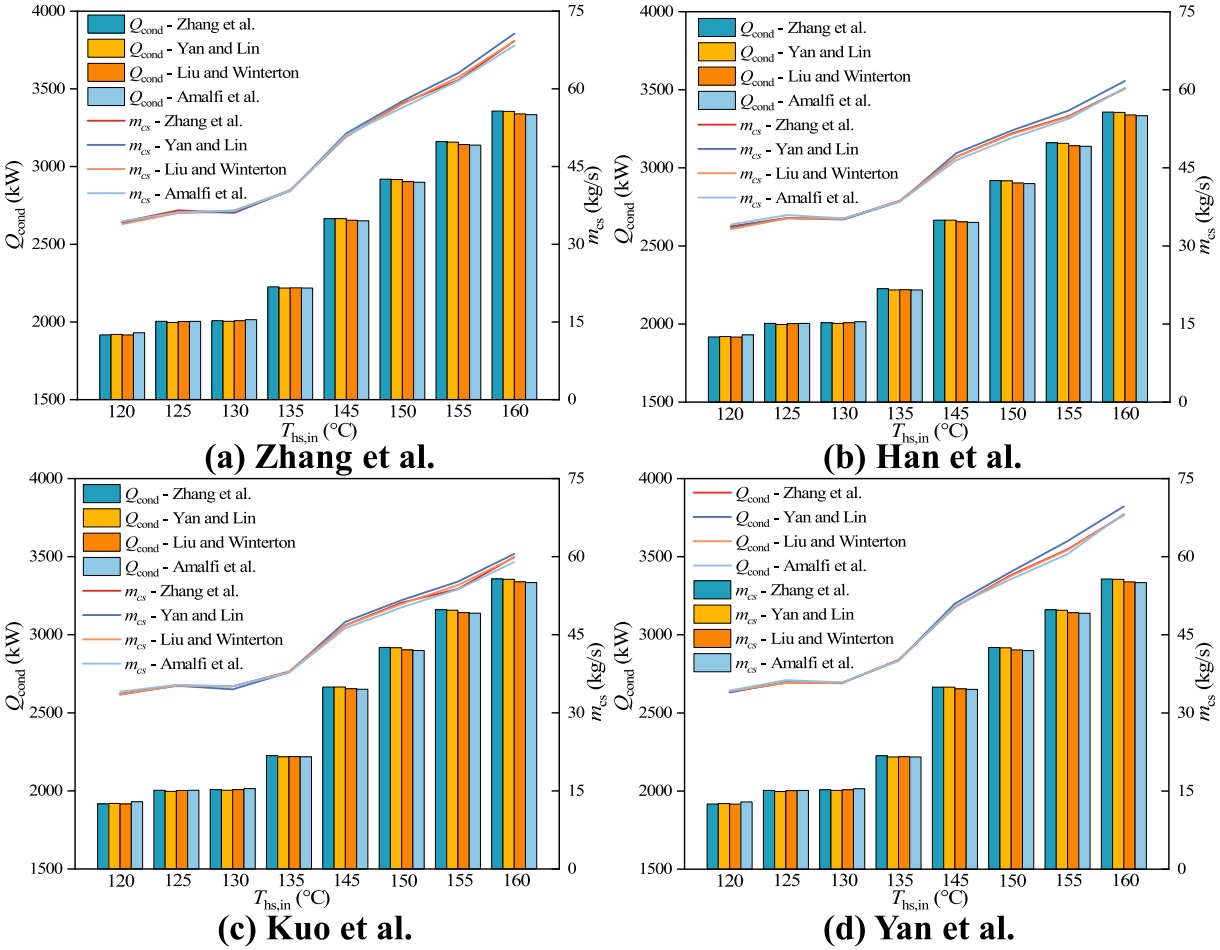

Fig. 16. Variation of Q_{cond} and m_{cs} with $T_{hs,in}$ among 4 flow boiling correlations under 4 fixed condensers.

satisfied to obtain a maximum net output power. To explain the existence of this optimal match, the variation trend of $T_{hs,out}$ and $T_{eva,out}$ at $T_{hs,in}$ = 125 °C is presented as an example in Fig. 15. (a). The $T_{hs,out}$ and $T_{eva,out}$ increase as the reduced pressure P_r rises. In this way the inlet temperature difference $\Delta T_{eva,in}$ rises and the outlet temperature difference $\Delta T_{eva,out}$ drops at the same time as shown in Fig. 15. (b). Therefore the ratio of $\Delta T_{ea,out}$ and $\Delta T_{eva,in}$ decline gradually as illustrated intuitively by Fig. 15. (b). The ascension of $\Delta T_{eva,in}$ will lead to the decrease of the temperature difference between the inlet and outlet for the heat source, which causes the heat transfer rate decrease of the evaporator according to eq. (9) and further results in the downward trend of the net output power. On the contrary, the decline of $\Delta T_{eva,out}$ leads to the increment of working fluid outlet temperature. In this way the enthalpy difference Δh_{turb} between the inlet and outlet of the expander increases which contributes to an upward trend for the net output power according to eqs. (5) and (11). Due to the effective influence from the decline of $\Delta T_{eva,out}$ and negative action from the ascension of $\Delta T_{eva,in}$, the maximum W_{net} will be obtained after a proper trade-off.

Under the off-design conditions, the working fluid status in the evaporator is influenced by the specific value of $T_{hs,in}$ while an optimal

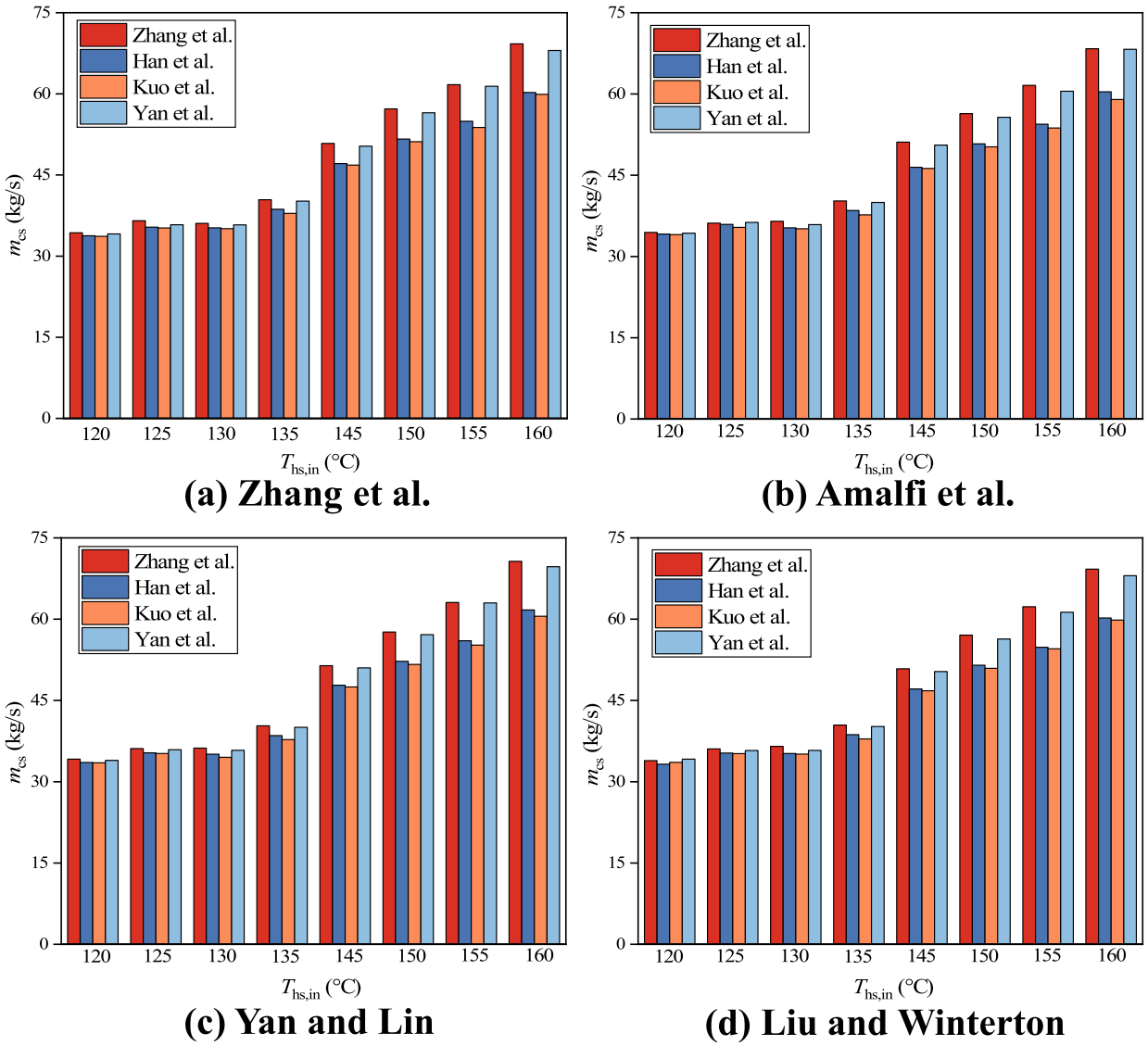

Fig. 17. Variation of m_{cs} with $T_{hs,in}$ among 4 flow condensation correlations under 4 fixed evaporators.

W_{net} is obtained. For the limitation of working fluid properties, the optimal W_{net} is achieved at the highest given reduced pressure of 0.96 in this paper when the value of $T_{hs,in}$ is above the design level. As for the cases when the value of $T_{hs,in}$ is under the design level, a proper balance between the effective influence of $\Delta T_{eva,out}$ and negative action of $\Delta T_{eva,in}$ should be made to get the maximum W_{net}.

As discussed above, the comparison of 4 flow boiling correlations shows little difference in W_{net} which has been shown clearly in Fig. 13. Hence in Fig. 16, the potential relation between 4 flow boiling correlations and ORC cooling performance is further discussed under each flow condensation correlation. To particularly discuss the influence of 4 flow condensation correlations in the ORC system, in Fig. 17 the cooling performance of the ORC system is presented under each flow boiling correlation.

As shown in Fig. 16, with the increase of $T_{hs,in}$ the cooling demand of the ORC system is rising and the difference among different flow boiling correlations is also indistinct which is similar to the relative difference of the maximum W_{net} calculated by different flow boiling correlations listed in Table 8. This inconspicuous distinction derives from the slight difference among the design results as shown in Fig. 9. Due to the similar size parameters of evaporators designed from 4 flow boiling correlations, similar heat transfer performance among different evaporators will be achieved, which further leads to the indistinct difference of the system performance. In addition, through comparing the cooling demand among different flow condensation correlations it is found that the variation pattern of the cooling capacity Q_{cond} nearly keeps no change. This is because the expander is simulated by a simplified theoretical calculation, which means the inlet status of the condenser is indirectly determined by the similar outlet states of the designed evaporators. Hence based on the definition of the ideal unified boundary in this paper the calculated net output power and cooling capacity will be close to each other as long as the difference among the designed evaporators is indistinct.

From the increasing trend of the cooling water mass flow m_{cs}, different behaviours among different flow condensation correlations can be found in Fig. 16, especially at $T_{hs,in} = 160$ °C. And the variation of m_{cs} with $T_{hs,in}$ among 4 flow condensation correlations under 4 fixed evaporators is shown in Fig. 17. It can still be recognized that among different flow boiling correlations, the overall variation characteristic keeps almost no change under a new perspective. When the heat source temperature is below 140 °C the difference of m_{cs} among 4 flow condensation correlations is still limited. With the increase of $T_{hs,in}$ the most obvious difference can be observed at $T_{hs,in} = 160$ °C. Considering the actual cooling capacity is the same, this obvious difference should be

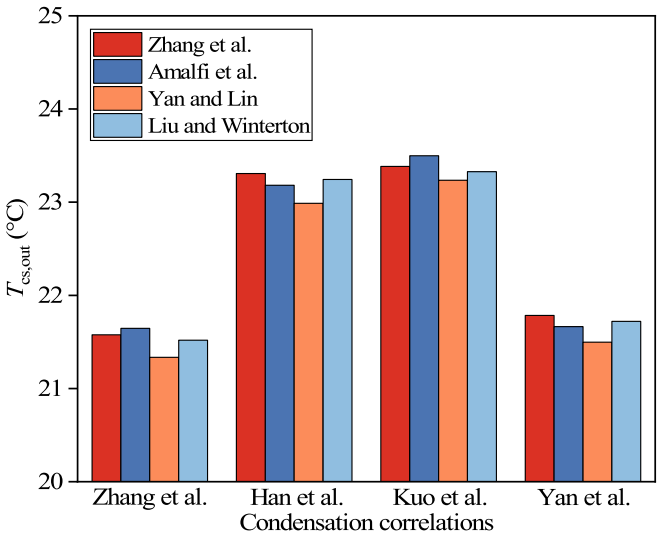

Fig. 18. Variation of $T_{cs,out}$ with correlations.

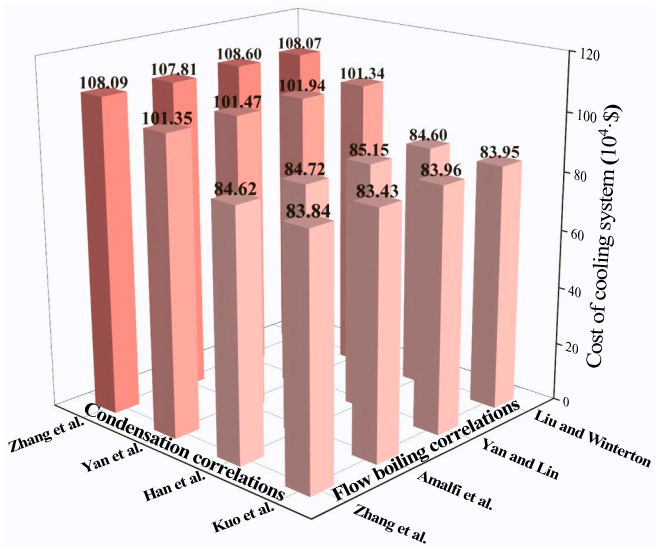

Fig. 19. Comparison of the cooling system cost.

caused by the different cooling performance behaviours among these 4 condensers. As presented in Fig. 10, the heat transfer area of the condenser designed by Zhang et al. correlation [19] is the largest and therefore the corresponding cooling water mass flow has to be high enough to satisfy the same cooling capacity by reducing the temperature increment of the cooling water as shown in Fig. 18.

3.3.2. *Comparative analysis of economic and environmental performance*

As the maximum net output power is achieved and the cooling performance demand distinction is also obvious at $T_{hs,in}$ = 160 °C, the following analysis of the economic and environmental performance is discussed based on this heat source condition. It has been discussed that from the perspective of components the difference of economic and environmental performance among condensers is more apparent than that among evaporators as displayed in Fig. 11 and Fig. 12. To further compare the system performance behaviours under different design correlations, the economic aspect is firstly focused. The cost of a cooling system consisting of a condenser, water pump, and cooling tower under 16 sorts of correlation combinations is presented in Fig. 19. It is clear that the cooling system cost changes a lot by varying the selection of the

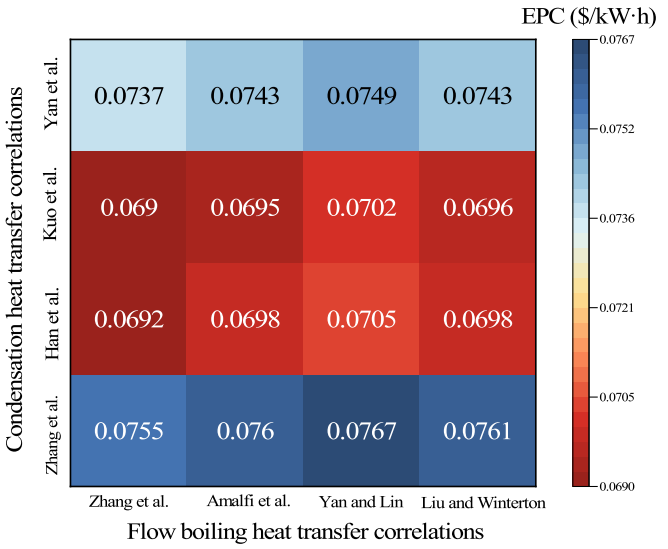

Fig. 20. Comparison of the ORC system *EPC*.

flow condensation correlations rather than the flow boiling correlations. Hence the cost evaluation of the cooling system is significantly affected by the selection of flow condensation correlations and this may lead to an incorrect budget for the realistic cooling system.

Moreover, the economic performance of the whole ORC system among 16 sorts of correlation combinations is shown in Fig. 20. The value of *EPC* ranges from 0.069 to 0.0767 and thus the maximum relative difference is 11.2%, which means the selection of design correlations also has a significant influence in the perspective of system economic performance.

As shown in Fig. 21, the ORC system environmental performance parameter GHG_{tot} ranges from 270.78 to 273.38 and the maximum relative difference is 0.96%, which displays a strong stabilization. From the comparative analysis above among various design correlations, the size distinction along with the heat transfer area difference among designed PHEs is the main reason leading to the thermodynamic and economic performance difference. While the variation of system GHG_{tot} is not obvious among 16 sorts of correlation combinations. This is because the definition of system GHG_{tot} considers the carbon emission not only from equipment manufactory and recycling but also from the working fluid cycling and leakage, which weakens the impact of different designed PHE sizes from different correlation combinations. Therefore, the selection of design correlations hardly influences the system's environmental performance evaluation.

4. Conclusions

A comparative study of the ORC thermodynamic, economic and environmental performance was conducted to investigate the influence of different heat exchanger design correlations. In this paper, the selected flow boiling correlations are the Zhang et al. correlation [16], the Yan and Lin correlation [10], the Liu and Winterton correlation [17], and the Amalfi et al. correlation [18]. The selected flow condensation correlations are the Zhang et al. correlation [19], the Yan et al. correlation [22], the Kuo et al. correlation [20], and the Han et al. correlation [21]. Based on the selected optimal working fluid R1234ze(E) along with the design working condition, in the perspective of components, the geometric size, economic and environmental performance difference among designed plate heat exchangers was discussed. Moreover, under off-design conditions, performance comparison analysis from the perspective of the system is carried out. The main conclusions can be illustrated as follows:

1) Considering the environmental protection demand, safety level

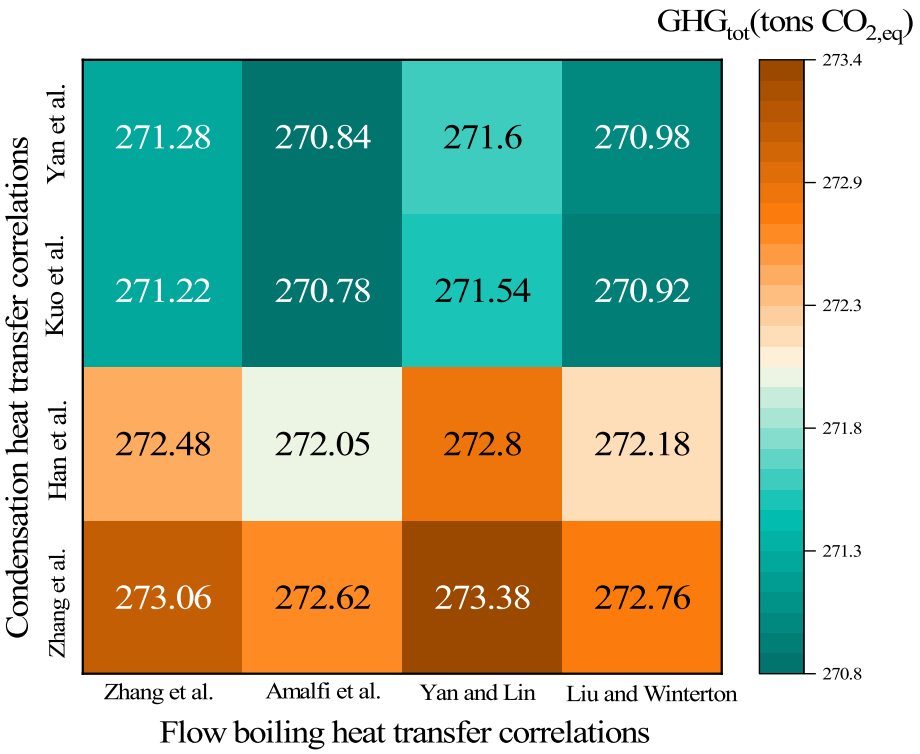

Fig. 21. Comparison of the ORC system GHG_{tot}.

and other properties, 5 working fluid candidates are picked out preliminarily. Based on the thermodynamic performance comparison, it is hard to find a working fluid with an all-around performance from the candidates. The fluid R1234ze(E) was selected as the optimal fluid which maximized the ORC system net output work.

2) Under the design condition, the size along with the economic and environmental performance of designed evaporators is finitely affected by different flow boiling correlations. However, an obvious difference among the designed condensers is obtained by utilizing different flow condensation correlations. The relative difference between the maximum predicted condenser plate length and the minimum one is up to 103.20%, which further leads to an unforeseeable uncertainty for the economic and environmental performance evaluation.

3) Under the off-design conditions, the thermodynamic performance of the ORC cycle changes significantly along with the heat source temperatures. Through the comparison of the maximum net output power, the influence of 4 flow boiling correlations is found to be slight with a relative difference within 1.1%. While the impact of 4 flow condensation correlations on the cooling system performance is more obvious as the heat source temperature increases.

4) The economic and environmental performance under the off-design conditions is compared under 16 sorts of correlation combinations. The cost evaluation of the cooling system is significantly affected by the flow condensation correlations which may lead to an incorrect budget of the cooling system. The selection of design correlations also has a significant influence on the system's economic performance and the maximum relative difference among values of *EPC* is 11.2%. While the environmental performance is hardly affected by different correlations with the parameter GHG_{tot} ranging from 270.78 to 273.38 and the maximum relative difference being 0.96%.

CRediT authorship contribution statement

Ji Zhang: Writing – review & editing, Writing – original draft, Methodology, Funding acquisition, Formal analysis, Conceptualization. **Xudong Hu:** Writing – review & editing, Methodology, Investigation, Formal analysis. **Ding Wu:** Writing – review & editing, Methodology, Investigation, Formal analysis. **Xiaohui Huang:** Writing – review & editing, Methodology, Investigation, Formal analysis. **Xuehui Wang:** Writing – review & editing. **Yan Yang:** Writing – review & editing, Supervision, Methodology, Formal analysis. **Chuang Wen:** Writing – review & editing, Supervision, Methodology, Investigation, Formal analysis.

Declaration of Competing Interest

The authors declare that they have no known competing financial interests or personal relationships that could have appeared to influence the work reported in this paper.

Data availability

Data will be made available on request.

Acknowledgements

The research presented in the paper has received fundings from Changsha Science and Technology Bureau (project ID: kq2202159) and National Key R&D Program of China (project ID: 2022YFE011925). The financial supports are gratefully acknowledged.

Appendix A

The economic model is described below. Taking the carbon steel construction and ambient operating pressure into consideration mainly, the cost of each piece of equipment in the ORC system is calculated by the following equations [53]

For the evaporator (the condenser is the same):

$$log_{10}C_{p,eva} = K_{1,eva} + K_{2,eva}log_{10}(A_{eva}) + K_{3,eva}[log_{10}(A_{eva})]^2 \quad (A.1)$$

For the working fluid pump (the cooling water pump is the same):

$$log_{10}C_{p,Fpump} = K_{1,Fpump} + K_{2,Fpump}log_{10}(W_{Fpump}) + K_{3,Fpump}[log_{10}(W_{Fpump})]^2 \quad (A.2)$$

For the turbine:

$$log_{10}C_{p,turb} = K_{1,turb} + K_{2,turb}log_{10}(W_{turb}) + K_{3,turb}[log_{10}(W_{turb})]^2 \quad (A.3)$$

where K_1, K_2, K_3, C_1, C_2, C_3 and are fitting cost coefficients, which are given in Table A.1.

Table A.1
Coefficients in capital cost models.

Equipment	K_1	K_2	K_3	C_1	C_2	C_3	B_1	B_2	F_m	F_{bm}
Evaporator	4.67	−0.156	0.155	0	0	0	0.96	1.21	1.0	/
Condenser	4.67	−0.156	0.155	0	0	0	0.96	1.21	1.0	/
Pumps	3.87	0.316	0.122	−0.245	0.259	−0.0136	1.89	1.35	1.5	/
Turbine	2.25	1.50	−0.162	/	/	/	/	/	/	3.3

When considering the specific material of equipment and operating pressure, the correction for bare module cost is presented as:

$$C_{BM} = C_p F_{bm} = C_p(B_1 + B_2 F_m F_p) \quad (A.4)$$

where B_1 and B_2 are fitting cost coefficients, F_m is the material correction factor, as given in Table A.1, F_p is the pressure correction factor and is determined by the following equation:

$$log_{10}F_p = C_1 + C_2 log_{10}(p) + C_3[log_{10}(p)]^2 \quad (A.5)$$

The cost of the cooling tower is calculated by the following Eq. [54], which is fitted via data from various models of different commercial products from manufacturers:

$$C_{BM,ctower} = 22.582Q_{cond} + 1924.6 \quad (A.6)$$

The cost calculated by the above formula is suitable for 2001, which should be converted to 2020 by the *CEPCI* (Chemical Engineering Plant Cost Index) via the following Eq. [55]:

$$C_{BM,2020} = \frac{C_{BM,2001} \cdot CEPCI_{2020}}{CEPCI_{2001}} \quad (A.7)$$

where $CEPCI_{2020} = 596.2$, $CEPCI_{2001} = 397$.

The total purchase cost consists of an evaporator, condenser, refrigerant pump, turbine, cooling water pump, and cooling tower, which can be approximately presented as:

$$C_{total} = C_{BM,eva} + C_{BM,cond} + C_{BM,Fpump} + C_{BM,turb} + C_{BM,cpump} + C_{BM,ctower} \quad (A.8)$$

The cooling system purchase cost consists of a condenser, cooling water pump, and cooling tower, which can be approximately presented as:

$$C_{cooling} = C_{BM,cond} + C_{BM,cpump} + C_{BM,ctower} \quad (A.9)$$

Furthermore, the *EPC* (electricity production cost) is calculated as:

$$EPC = \frac{(C_{total}CRF + COM)}{t_{op}W_{net}} \quad (A.10)$$

where the t_{op} denotes the operating time per year and is set as 8000 h, *COM* and *CRF* are the cost of operation and maintenance and the capital recovery factor respectively:

$$COM = 0.016C_{total} \quad (A.11)$$

$$CRF = \frac{i(1+i)^{LT}}{[(1+i)^{LT} - 1]} \quad (A.12)$$

where i is the annual loan interest rate and is set as 5%, LT denotes the life cycle time and is set as 15 years.

Appendix B

The environmental model is described below. The global warming impact of the ORC system is measured by GHG (greenhouse gas), which is a summation of equivalent carbon dioxide emissions of a product or service across its life cycle. As shown in Fig. B.1, the components of the total GHG

include direct emissions and indirect emissions [56]

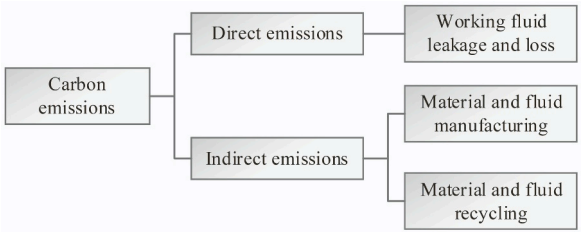

Fig. B.1. Carbon emissions categories.

The direct emission result from working fluid leakage and loss, including annual leakage during the operation and working fluid loss when the system is disposed of:

$$GHG_{\text{direct}} = M_{\text{fc}} \times \varphi_{\text{ALR}} \times GWP \times LT + M_{\text{fc}} \times \varphi_{\text{EOL}} \times GWP \tag{B.1}$$

where M_{fc} is the quality of fluid charged in ORC, φ_{ALR} is the annual leak rate of working fluid which is set as 5% according to refrigeration industry regulations [57]. *GWP* is the global warming potential parameter of the working fluid and for R1234ze(E) the value of the GWP is 1 in this paper. What's more, φ_{EOL} represents the end-of-life loss rate set as 15% [57].

The indirect emissions result from the manufacturing and recycling process of the material and working fluid:

$$GHG_{\text{indirect}} = \sum_{i=1}^{n} M_{\text{material,i}} \times \alpha_{\text{MM,i}} + \sum_{i=1}^{n} M_{\text{material,i}} \times \alpha_{\text{MR,i}} + M_{\text{fc}}(1 + LT \times \varphi_{\text{ALR}}) \times \alpha_{\text{FM}} + M_{\text{fc}} \times (1 - \varphi_{\text{EOL}}) \times \alpha_{\text{FD}} \tag{B.2}$$

where $M_{material,i}$ is the quality of *i*-th material, $\alpha_{MM,i}$ and $\alpha_{MR,i}$ are the coefficients that reflect the GHG emissions from manufacturing and recycling processes of *i*-th unit material, while α_{FM} and α_{FD} reflect the GHG emissions produced from working fluid manufacturing and disposal processes.All the equipment's materials are set as steel, thus $\alpha_{MM} = 2.46$ kg $CO_{2,eq}$/kg, $\alpha_{MR} = 0.07$ kg $CO_{2,eq}$/kg. The selected working fluids is R1234ze(E), therefore, $\alpha_{FM} = 13.7$ kg $CO_{2,eq}$/kg, $\alpha_{FR} = 1.16$ kg $CO_{2,eq}$/kg.

The quality of the working fluid R1234ze(E) M_{fc} is set as 7.36 t. The quality of the material in ORC is determined by the following equations:

For the evaporator (the condenser is the same):

$$m_{\text{evap,steel}} \approx \rho V_{\text{evap}} = \rho \delta A_{\text{evap}} \tag{B.3}$$

For the working fluid pump:

$$m_{\text{Fpump}} \approx 14 \cdot W_{\text{Fpump}} \tag{B.4}$$

For the turbine:

$$m_{\text{tur}} \approx 31.22 \cdot W_{\text{tur}} \tag{B.5}$$

References

[1] Dadpour D, Gholizadeh M, Lakzian E, Delpisheh M, Kim HD. Vehicle refrigeration modification using an ejector: optimization and exergoeconomic analysis. J Taiwan Inst Chem Eng 2023;148:104875. https://doi.org/10.1016/j.jtice.2023.104875.

[2] Khodadadi F, Deymi-Dashtebayaz M, Lakzian E. Parametric analysis of combined power and freshwater producing system for natural gas engine heat recovery. Energ Conver Manage 2020;225:113464. https://doi.org/10.1016/j.enconman.2020.113464.

[3] Zhu Q, Pishahang M, Bichnevicius M, Amy C, Caccia M, Sandhage KH, et al. The importance of maldistribution matching for thermal performance of compact heat exchangers. Appl Energy 2022;324:119576. https://doi.org/10.1016/j.apenergy.2022.119576.

[4] Luo J, Lu P, Chen K, Luo X, Chen J, Liang Y, et al. Experimental and simulation investigation on the heat exchangers in an ORC under various heat source/sink conditions. Energy 2023;264:126189. https://doi.org/10.1016/j.energy.2022.126189.

[5] Joy J, Chowdhury K. Appropriate number of stages of an ORC driven by LNG cold energy to produce acceptable power with reasonable surface area of heat exchangers. Cryogenics 2022;128:103599. https://doi.org/10.1016/j.cryogenics.2022.103599.

[6] Blondel Q, Tauveron N, Lhermet G, Caney N. Zeotropic mixtures study in plate heat exchangers and ORC systems. Appl Therm Eng 2023;219:119418. https://doi.org/10.1016/j.applthermaleng.2022.119418.

[7] Hsieh YY, Lin TF. Saturated flow boiling heat transfer and pressure drop of refrigerant R-410A in a vertical plate heat exchanger. Int J Heat Mass Transfer 2002;45(5):1033–44. https://doi.org/10.1016/S0017-9310(01)00219-8.

[8] Caputo AC, Federici A, Pelagagge PM, Salini P. On the design of shell-and-tube heat exchangers under uncertain operating conditions. Appl Therm Eng 2022;212:118541. https://doi.org/10.1016/j.applthermaleng.2022.118541.

[9] Han DH, Lee KJ, Kim YH. Experiments on the characteristics of evaporation of R410A in brazed plate heat exchangers with different geometric configurations. Appl Therm Eng 2003;23:1209–25. https://doi.org/10.1016/S1359-4311(03)00061-9.

[10] Yan Y-Y, Lin T-F. Evaporation Heat Transfer and Pressure Drop of Refrigerant R-134a in a Plate Heat Exchanger. Int J Heat Mass Transf 1999;121(1):118–27. https://doi.org/10.1115/1.2825924.

[11] Lambert J, Gosselin L. Sensitivity analysis of heat exchanger design to uncertainties of correlations. Appl Therm Eng 2018;136:531–40. https://doi.org/10.1016/j.applthermaleng.2018.03.037.

[12] Chatzopoulou MA, Lecompte S, De Paepe M, Markides CN. Off-design optimisation of organic Rankine cycle (ORC) engines with different heat exchangers and volumetric expanders in waste heat recovery applications. Appl Energy 2019;253:113442. https://doi.org/10.1016/j.apenergy.2019.113442.

[13] Liu C, Gao T. Off-design performance analysis of basic ORC, ORC using zeotropic mixtures and composition-adjustable ORC under optimal control strategy. Energy 2019;171:95–108. https://doi.org/10.1016/j.energy.2018.12.195.

[14] Du Y, Han P, Qiang X, Hao M, Long Y, Zhao P, et al. Off-design performance analysis of a combined cooling and power system driven by low-grade heat source. Energ Conver Manage 2018;159:327–41. https://doi.org/10.1016/j.enconman.2017.12.076.

[15] Chatzopoulou MA, Lecompte S, De Paepe M, Markides CN. Off-design optimisation of organic Rankine cycle (ORC) engines with different heat exchangers and volumetric expanders in waste heat recovery applications. Appl Energy 2019;253:113442. https://doi.org/10.1016/j.apenergy.2019.113442.

[16] Zhang J, Haglind F. Experimental analysis of high temperature flow boiling heat transfer and pressure drop in a plate heat exchanger. Appl Therm Eng 2021;196:117269. https://doi.org/10.1016/j.applthermaleng.2021.117269.

[17] Liu Z, Winterton R. A general correlation for saturated and subcooled flow boiling in tubes and annuli, based on a nucleate pool boiling equation. Int J Heat Mass Transf 1991;34(11):2759–66. https://doi.org/10.1016/0017-9310(91)90234-6.
[18] Amalfi RL, Vakili-Farahani F, Thome JR. Flow boiling and frictional pressure gradients in plate heat exchangers. Part 2: Comparison of literature methods to database and new prediction methods. Int J Refrig 2016;61:185–203. https://doi.org/10.1016/j.ijrefrig.2015.07.009.
[19] Zhang J, Kærn MR, Ommen T, Elmegaard B, Haglind F. Condensation heat transfer and pressure drop characteristics of R134a, R1234ze(E), R245fa and R1233zd(E) in a plate heat exchanger. Int J Heat Mass Transf 2019;128:136–49. https://doi.org/10.1016/j.ijheatmasstransfer.2018.08.124.
[20] Kuo WS, Lie YM, Hsieh YY, Lin TF. Condensation heat transfer and pressure drop of refrigerant R-410A flow in a vertical plate heat exchanger. Int J Heat Mass Transf 2005;48(25–26):5205–20. https://doi.org/10.1016/j.ijheatmasstransfer.2005.07.023.
[21] Han D-H, Lee K-J, Kim Y-H. The Characteristics of Condensation in Brazed Plate Heat Exchangers with Different Chevron Angles. J. Korean Phys. Soc 2003;43(1):66–73. https://doi.org/10.1016/S0022-3697(03)00042-8.
[22] Yan YY, Lio HC, Lin TF. Condensation heat transfer and pressure drop of refrigerant R-134a in a plate heat exchanger. Int J Heat Mass Transf 1999;42(6):993–1006. https://doi.org/10.1016/S0017-9310(98)00217-8.
[23] Altun AF, Kilic M. Thermodynamic performance evaluation of a geothermal ORC power plant. Renew Energy 2020;148:261–74. https://doi.org/10.1016/j.renene.2019.12.034.
[24] Chitgar N, Hemmati A, Sadrzadeh M. A comparative performance analysis, working fluid selection, and machine learning optimization of ORC systems driven by geothermal energy. Energ Conver Manage 2023;286:117072. https://doi.org/10.1016/j.enconman.2023.117072.
[25] Zhao Z, Luo J, Zou D, Yang K, Wang Q, Chen G. Experimental investigation on the inhibition of flame retardants on the flammability of R1234ze(E). Energy 2023;263:126149. https://doi.org/10.1016/j.energy.2022.126149.
[26] Başaran A. Experimental investigation of R600a as a low GWP substitute to R134a in the closed-loop two-phase thermosyphon of the mini thermoelectric refrigerator. Appl Therm Eng 2022;211:118501. https://doi.org/10.1016/j.applthermaleng.2022.118501.
[27] Yang MH, Yeh RH. The effects of composition ratios and pressure drops of R245fa/R236fa mixtures on the performance of an organic Rankine cycle system for waste heat recovery. Energ Conver Manage 2018;175:313–26. https://doi.org/10.1016/j.enconman.2018.09.006.
[28] Zhang J, Zhu X, Mondejar ME, Haglind F. A review of heat transfer enhancement techniques in plate heat exchangers. Renew Sustain Energy Rev 2019;101:305–28. https://doi.org/10.1016/j.rser.2018.11.017.
[29] Chen Q, Xu J, Chen H. A new design method for Organic Rankine Cycles with constraint of inlet and outlet heat carrier fluid temperatures coupling with the heat source. Appl Energy 2012;98:562–73. https://doi.org/10.1016/j.apenergy.2012.04.035.
[30] Cooper MG. Flow boiling-the 'apparently nucleate' regime. Heat Mass Transf 1989;32(3):459–64. https://doi.org/10.1016/0017-9310(89)90133-6.
[31] Incropera FP, DeWitt DP, Bergman TL, Lavine AS. Fundamentals of heat and mass transfer. John Wiley & Sons; 1996.
[32] Cooper MG. Saturation nucleate pool boiling - a simple correlation. The Institution of Chemical Engineers Symposium Series 1984;(86):785–93. https://doi.org/10.1016/B978-0-85295-175-0.50013-8.
[33] Danilova GN, Azarskov VM, Zemskov BB. Heat transfer in plate evaporators of different geometry. Kholod. Tek 1981;4:25–31.
[34] Huang J, Sheer TJ, Bailey-Mcewan M. Heat transfer and pressure drop in plate heat exchanger refrigerant evaporators. Int J Refrig 2012;35:325–35. https://doi.org/10.1016/j.ijrefrig.2011.11.002.
[35] Donowski VD, Kandlikar SG. Correlating evaporation heat transfer coefficient of refrigerant R-134aIN A plate heat exchanger. J Heat Transf 1999;121:118–27. https://doi.org/10.1115/1.2825924.
[36] Zhang J, Desideri A, Kærn MR, Ommen TS, Wronski J, Haglind F. Flow boiling heat transfer and pressure drop characteristics of R134a, R1234yf and R1234ze in a plate heat exchanger for organic Rankine cycle units. Int J Heat Mass Transf 2017;108:1787–801. https://doi.org/10.1016/j.ijheatmasstransfer.2017.01.026.
[37] Xu J, Luo X, Chen Y, Mo S. Multi-criteria design optimization and screening of heat exchangers for a subcritical ORC. Energy Procedia 2015;75:1639–45. https://doi.org/10.1016/j.egypro.2015.07.397.
[38] Sène P, Giraud F, Sow ML, Tréméac B. Heat transfer coefficient correlations of water subatmospheric vaporization in a channel of a smooth plate heat exchanger, based on Vaschy-Buckingham theorem. Appl Therm Eng 2022;213:118800. https://doi.org/10.1016/j.applthermaleng.2022.118800.
[39] Blondel Q, Tauveron N, Lhermet G, Caney N. Zeotropic mixtures study in plate heat exchangers and ORC systems. Appl Therm Eng 2023;219:119418. https://doi.org/10.1016/j.applthermaleng.2022.119418.
[40] Hagen BAL, Nikolaisen M, Andresen T. A novel methodology for Rankine cycle analysis with generic heat exchanger models. Appl Therm Eng 2020;165:114566. https://doi.org/10.1016/j.applthermaleng.2019.114566.
[41] Kutateladze SS. Boiling heat transfer. Int J Heat Mass Transf 1961;4:31–45. https://doi.org/10.1016/0017-9310(61)90059-X.
[42] Kandlikar SG. A general correlation for saturated two-phase flow boiling heat transfer inside horizontal and vertical tubes. ASME J Heat Transf 1990;112:219–28. https://doi.org/10.1115/1.2910348.
[43] Lu P, Luo X, Wang J, Chen J, Liang Y, Yang Z, et al. Thermo-economic design, optimization, and evaluation of a novel zeotropic ORC with mixture composition adjustment during operation. Energ Conver Manage 2021;230:113771. https://doi.org/10.1016/j.enconman.2020.113771.
[44] Liu C, Gao T. Off-design performance analysis of basic ORC, ORC using zeotropic mixtures and composition-adjustable ORC under optimal control strategy. Energy 2019;171:95–108. https://doi.org/10.1016/j.energy.2018.12.195.
[45] Martin H. A theoretical approach to predict the performance of chevron-type plate heat exchangers. Chem Eng Process: Process Intensif 1996;35(4):301–10. https://doi.org/10.1016/0255-2701(95)04129-X.
[46] Chatzopoulou MA, Lecompte S, De Paepe M, Markides CN. Off-design optimisation of organic Rankine cycle (ORC) engines with different heat exchangers and volumetric expanders in waste heat recovery applications. Appl Energy 2019;253:113442. https://doi.org/10.1016/j.apenergy.2019.113442.
[47] Pereira JS, Ribeiro JB, Mendes R, André JC. Analysis of a hybrid (topping/bottoming) ORC based CHP configuration integrating a new evaporator design concept for residential applications. Appl Therm Eng 2019;160:113984. https://doi.org/10.1016/j.applthermaleng.2019.113984.
[48] El-Emam RS, Dincer I. Exergy and exergoeconomic analyses and optimization of geothermal organic Rankine cycle. Appl Therm Eng 2013;59:435–44. https://doi.org/10.1016/j.applthermaleng.2013.06.005.
[49] Jiang J, Li C, Kong M, Ye X. Insights into 4E evaluation of a novel solar-assisted gas-fired decarburization power generation system with oxygen-enriched combustion. Energy 2023;278:127771. https://doi.org/10.1016/j.energy.2023.127771.
[50] Satanphol K, Pridasawas W, Suphanit B. A study on optimal composition of zeotropic working fluid in an Organic Rankine Cycle (ORC) for low grade heat recovery. Energy 2017;123:326–39. https://doi.org/10.1016/j.energy.2017.02.024.
[51] Wang S, Liu C, Zhang S, Li Q, Huo E. Multi-objective optimization and fluid selection of organic Rankine cycle (ORC) system based on economic-environmental-sustainable analysis. Energ Conver Manage 2022;254:115238. https://doi.org/10.1016/j.enconman.2022.115238.
[52] Zhang C, Liu C, Xu X, Li Q, Wang S. Energetic, exergetic, economic and environmental (4E) analysis and multi-factor evaluation method of low GWP fluids in trans-critical organic Rankine cycles. Energy 2019;168:332–45. https://doi.org/10.1016/j.energy.2018.11.104.
[53] Zhang C, Liu C, Wang S, Xu X, Li Q. Thermo-economic comparison of subcritical organic Rankine cycle based on different heat exchanger configurations. Energy 2017;123:728–41. https://doi.org/10.1016/j.energy.2017.01.132.
[54] Usman M, Imran M, Yang Y, Lee DH, Park BS. Thermo-economic comparison of air-cooled and cooling tower based Organic Rankine Cycle (ORC) with R245fa and R1233zde as candidate working fluids for different geographical climate conditions. Energy 2017;123:353–66. https://doi.org/10.1016/j.energy.2017.01.134.
[55] Wang S, Liu C, Zhang S, Li Q, Huo E. Multi-objective optimization and fluid selection of organic Rankine cycle (ORC) system based on economic-environmental-sustainable analysis. Energ Conver Manage 2022;254:115238. https://doi.org/10.1016/j.enconman.2022.115238.
[56] Zhang C, Liu C, Xu X, Li Q, Wang S. Energetic, exergetic, economic and environmental (4E) analysis and multi-factor evaluation method of low GWP fluids in trans-critical organic Rankine cycles. Energy 2019;168:332–45. https://doi.org/10.1016/j.energy.2018.11.104.
[57] Hwang Y, Ferreira CI, Piao CC. Guideline for life cycle climate performance International Institute of Refrigeration. 2015.